THE UNIVERSITY OF WESTERN ONTARIO
DEPARTMENT OF CIVIL AND
ENVIRONMENTAL ENGINEERING

Water Resources Research Report

Development of Probability Based Intensity-Duration-Frequency Curves under Climate Change

By:
Tarana A. Solaiman
and
Slobodan P. Simonovic

Report No: 072
Date: March 2011

Development of Probability Based Intensity-Duration-Frequency Curves under Climate Change

By:

Tarana A. Solaiman

And

Slobodan P. Simonovic

Department of Civil and Environmental Engineering

The University of Western Ontario

London, Ontario, Canada

March 2011

Executive Summary

Hydrologic design of storm sewers, culverts, retention/detention basins and other components of storm water management systems are typically performed based on specified design storms derived from the rainfall intensity-duration-frequency (IDF) estimates and an assumed temporal distribution of rainfall. Use of inappropriate data or design storms could lead to malfunctions of the infrastructure systems: over-estimation may result in costly over-design or under-estimation may be associated with risk and human safety. One of the expected hydro-climatic impacts of climate change for London is the increase in the magnitude and frequency of extreme rainfalls which can have serious impact on the design, operation and maintenance of existing municipal water infrastructure.

This study presents a methodology for updating the rainfall IDF curves for the City of London incorporating various uncertainties associated with the assessment of climate change impacts on a local scale. Overall, two objectives have been achieved: first, an extensive investigation of the possible realizations of future climate from 29 scenarios developed from Atmosphere-Ocean Global Climate Models (AOGCM) and scenarios are performed using a downscaling based disaggregation approach. Annual maximum series of rainfall are fitted to Gumbel distribution to develop IDF curves for 1, 2, 6, 12 and 24 hour durations for 2, 5, 10, 25, 50 and 100 years of return periods. Next, the associated uncertainties are estimated using non-parametric kernel estimation approach and the resultant IDF curve is developed based on a probabilistic approach.

The results indicate that rainfall patterns in the City of London will most certainly change in future due to climate change. The use of the multi-model approach, rather than a single scenario

is encouraged. Inherent uncertainties associated with different AOGCMs are quantified by a kernel based plug-in estimation approach. The resultant scenario indicates approximately 20-40% changes in different duration rainfalls for all return periods. Use of a probability based intensity-duration-frequency curve is encouraged in order to apply the updated IDF information with higher level of confidence.

Table of Contents

List of Tables

List of Figures

1. Introduction

1.1 Problem Definition

The increase of carbon dioxide concentration in the atmosphere due to industrial activities in the past and recent times has been identified as the major cause of global warming and climate change. The normal balance of Earth's hydrological cycle has been altered due to the changes in the temperature and precipitation patterns. Projections from climate models suggest that the probability of occurrence of intense rainfall in future will increase due to the increase in green house gas emission (Mailhot and Duchesne, 2010). Research related to the analysis of extreme precipitation indices have projected an increase in the annual total precipitation during the second half of the past century; the number of days with precipitation is also expected to increase, with no consistent pattern for extreme wet events (Vincent and Mekis, 2005). Stone et al. (2000) reported seasonally increasing trends in total precipitation during the 20th century for southern parts of Canada resulting from increased heavy and intermediate events. Research related to the Upper Thames River basin (Solaiman and Simonovic, 2011) have also indicated that there is now higher probability that the occurrence of extreme precipitation events will be more frequent in future. Such changes in extreme events have enormous ecological, societal and economic impacts in the form of floods, droughts, heat waves, summer and ice storms and have great implications for municipalities: a small shift in the climate normals can have large consequences on the existing infrastructure; climate change will affect any municipalities (big or small, rural or urban) by damaging existing municipal infrastructure (bridges/roads), natural systems (watersheds, wetlands and forests) and human system (health and education) (Mehdi et al, 2006). The design standards at present are based on the historic climate information and required level of protection from natural phenomena. Under a changing climate, it has become a

priority for the municipalities to search for appropriate procedures, planning and management to deal with and adopt to changing climatic conditions. Decision makers and stakeholders need to understand the possible effects for developing suitable management decisions for the future. Possible changes may demand new regulations, guidelines for storm water management studies, revision and update of design practices and standards, or retrofitting of existing infrastructure or even constructing additional ones (Prodanovic and Simonovic, 2007).

Global scale climate variables are commonly projected by Coupled Atmosphere-Ocean Global Climate Models (AOGCMs) to provide a numerical representation of the climate system based on the physical, chemical and biological properties of their components and feedback interactions between them (IPCC, 2007). They are, currently the most reliable tools available for obtaining the physics and chemistry of the atmosphere and oceans and to derive projections of meteorological variables (temperature, precipitation, wind speed, solar radiation, humidity, pressure, etc). They are based on various assumptions about the effects of the concentration of greenhouse gases in the atmosphere coupled with projections of CO_2 emission rates (Smith et al., 2009).

There is a high level of confidence that AOGCMs are able to capture large scale circulation patterns and correctly model smoothly varying fields such as surface pressure, especially at continental or larger scales. However, it is extremely unlikely that these models properly reproduce highly variable fields, precipitation (Hughes and Guttorp, 1994), on a regional scale, let alone, for small to medium watersheds. Although confidence has increased in the ability of AOGCMs to simulate extreme events, such as hot and cold spells, the frequency and the amount of precipitation during intense events are still being underestimated.

Present study aims to provide an insight into the future changes in the intensity of extreme rainfall events associated with model and scenario uncertainties and suggest methods for quantifying these uncertainties. The result is presented in the form of probability based intensity-duration-frequency (IDF) curves appropriate for the future climatic conditions.

1.2 Uncertainties in Atmosphere-Ocean Global Climate Models

In recent years, quantifying uncertainties from AOGCMs and scenarios for impact assessment studies has been identified as a critical climate change and adaptation research topic. Climate change impact studies derived from AOGCM outputs are associated with uncertainties due to "incomplete" knowledge originating from insufficient information or understanding of biophysical processes or a lack of analytical resources. Examples include simplification of complex processes involved in atmospheric and oceanographic transfers, inaccurate assumptions about climatic processes, limited spatial and temporal resolution resulting in a disagreement between AOGCMs over regional climate change, etc. Uncertainties also emerge due to "unknowable" knowledge arising from the inherent complexity of the Earth system and from our inability to forecast future socio-economic and human behavior in a deterministic manner (New and Hulme, 2000; Allan and Ingram, 2002; Proudhomme et al., 2003; Wilby and Harris, 2006; Stainforth et al., 2007; IPCC, 2007, Buytaert et al, 2009). It is now established that the accuracy of AOGCMs decrease at finer spatial and temporal scales; a typical resolution of AOGCMs ranges from 250 km to 600 km, but the need for impact studies conversely increase at finer scales. The representation of regional precipitation is distorted due to the coarse resolution and cannot capture the subgrid-scale processes significant for the formation of site-specific precipitation conditions. While some models are parameterized, details of the land-water distribution or topography in others are not represented at all (Widmann et al., 2003). Studies

have found that the models failed to predict the high variability in daily precipitation and could not accurately simulate present-day monthly precipitation amounts (Trigo and Palutikof, 2001; Brissette et al., 2006).

1.3 Intensity-Duration-Frequency Curves

Reliable rainfall intensity estimates are necessary for hydrologic analyses, planning and design problems. The rainfall intensity-duration-frequency (IDF) curve is one of the most common tools for urban drainage designer. Information from IDF curves are used to describe the frequency of extreme rainfall events of various intensity and durations. According to the guideline for 'Development, Interpretation and Use of Rainfall Intensity-Duration-Frequency (IDF) Information: A Guideline for Canadian Water Resources Practitioners" developed by Canadian Standards Association (CSA, 2010), the major reasons for increased demand for rainfall IDF information can be summarized as follows:

- *As the spatial heterogeneity of extreme rainfall patterns becomes better understood and documented, a stronger case is made for the value of "locally relevant" IDF information.*

- *As urban areas expand, making watersheds generally less permeable to rainfall and runoff, many older water systems fall increasingly into deficit, failing to deliver the services for which they were designed. Understanding the full magnitude of this deficit requires information on the maximum inputs (extreme rainfall events) with which drainage works must contend.*

- *Climate change will likely result in an increase in the intensity and frequency of extreme precipitation events in most regions in the future. As a result, IDF values will optimally need to be updated more frequently than in the past and climate change scenarios might eventually be drawn upon in order to inform IDF calculations.*

The typical establishment of rainfall IDF curves involves three steps. First a probability distribution function (PDF) or Cumulative Distribution Function (CDF) is fitted to each group comprised of the data value for any specific duration. The maximum rainfall intensity for each time interval is related with the corresponding return period from the cumulative distribution function. For a given return period T, the cumulative frequency F can be expressed as:

$$F = 1 - \frac{1}{T} \qquad (1.1)$$

or

$$T = \frac{1}{1-F} \qquad (1.2)$$

If the cumulative frequency is known, the maximum rainfall intensity can be determined using an appropriate theoretical distribution function (such as Generalized Extreme Value (GEV), Gumbel, Pearson Type III, etc).

In the presence of climate change, the theoretical distribution based on historical observations will be different for the future conditions. The issue is further aggravated by the presence of various uncertainties associated with AOGCM models and emission scenarios. Therefore, in this study the non-parametric kernel estimator is used to combine uncertainties generated from different AOGCMs. Probability of occurrences of maximum rainfall generated for any specific duration is presented in the form of cumulative distribution function for different return periods.

1.4 Outline of the Report

The report is organized as follows: research related to IDF information under climate is presented in Chapter 2. Chapter 3 details the database and methodology applied in the study. The

results and discussion obtained from the analysis are explained in Chapter 4. Finally the report

ends with conclusions based on the research findings.

2. Literature Review

Literature related to intensity-duration-frequency (IDF) curves concentrates on developing appropriate distribution of fit, comparison of sampling techniques and generation of IDF information under climate change.

Interesting research is emerging on the development of alternative methods, other than the distribution fit, for developing IDF values. Huard et al (2010) applied a Bayesian analysis to the estimation of IDF curves. Comparison of the Bayesian and classical approach using GEV distribution using Peak Over Threshold (POT) method indicated the extent of uncertainties in the IDF curves. Svensson et al (2007) made an experimental comparison of methods for estimating rainfall IDF from fragmented records for Eskdalemuir, Scotland. Three different methods were applied to cope with the missing data in the annual and monthly series: (i) using only years/months with complete records; (ii) using only years/months with complete records with not more than 20% missing data; and (iii) using censored data from months where records are incomplete. The result recommends the use of monthly maxima for calculating return period rainfall allowing up to 20% of missing data in each month. Despite the fact that over a decade long research have been investigating for alternate methods for IDF development, studies related to developing IDF curves incorporating climate change are limited.

Estimations of future modifications in rainfall due to increase in greenhouse gas concentrations depend on response from global climate models. Studies have related statistical downscaling with outputs from global and regional climate model outputs. Nguyen et al (2007a, b) and Desramaut (2008) presented a spatial-temporal downscaling method based on scale invariance technique for constructing IDF relations using outputs from two GCMs (HadCM3 A2

and CGCM2 A2) for future climate. The spatial downscaling methodology based on SDSM was used to generate daily precipitation data. The temporal scaling was performed for extreme value distribution factors based on current historical rainfall distribution. The studies found large differences in future IDF values between two the models.

Prodanovic and Simonovic (2007) developed IDF curves for current and future climate for city of London using a K-NN based weather generator. Future rainfall derived for the wet (CCSRNIES B21) scenario projected 30% increase in rainfall magnitude for a range of durations and return periods. More recently Simonovic and Peck (2009) used all the available precipitation data for different durations for developing IDF information under the wet climate change scenario. The 24 hr duration rainfall was modified by applying moving window procedure to recreate maximum 24 hour rainfall events crossing the calendar day boundary. Their study indicated 10.7% to 34.9% change in IDF information for 2050s.

Coulibaly and Shi (2005) used outputs from CGCM2 B2 to develop IDF curves for Grand River and Kenora Rainy River regions in Ontario using statistical SDSM downscaling methodology. Their study found an increase in the range of 24-35% in the rainfall intensity for 24 hour and sub-daily durations for all stations of interest for 2050s and 2080s with decreases in 2020s.

Mailhot et al. (2006, 2007) used outputs from Regional Climate Models (RCMs) (CRCM A2) for developing IDF for different durations for May-October over Southern Quebec using regional frequency analysis. The results were obtained for the RCM grid-box scale ranging over 45 km distances in between two grids. Projected rainfall showed 50% decrease by 2050s for 2 and 6 hour durations and 32% decrease for 12 and 24 hour durations than the base climate (1961-

1990). The results indicated limitation of using grid box scale and acknowledged that the results may be improved by using point estimates.

Onof and Arnbjeg-Nielsen (2009) used an hourly weather generator approach with disaggregation to derive IDF values from hourly rainfall data. Future hourly data was obtained from RCM A2 scenario with a 10 KM x 10 KM resolution for 2050s. The limitation of the study includes the stationarity assumption that the ratio of areal to the point estimates will remain unchanged with any changes in the climate.

Literature related to developing IDF values incorporating climate change from AOGCM models suffer from:

(i) *Limitations of statistical downscaling approaches:* Downscaling approaches such as SDSM or most of the weather generators assumed to have stationary climate. One possible way to overcome such issue is to perturb the model to generate values to achieve outputs beyond the range of inputs, which can be easily included in the weather generator.

(ii) *Application of sub-daily scaling factors to daily precipitation data and uncertainties:* Use of historical hourly data can prevent this issue.

(iii) *Use of single AOGCM response:* In all the literature listed above, single AOGCMs have been used for predicting future climate. It is well understood that in the presence of significant uncertainties, utilization of a single AOGCM may be one of all possible realizations and cannot be representative of the future. So, for a comprehensive assessment of the future changes, it is important to use collective information by utilizing all available GCM models, synthesizing the projections and uncertainties in a probabilistic manner.

(iv) *Appropriate distribution fit for future:* In presence of human induced warming trends added to Earth's natural variability, it is unlikely that the present precipitation or rainfall pattern

will comply with the future. Differences in the initializations and parameterizations of different climate model responses make it more complex to assume a specific distribution for all possible realizations.

3. Methodology

3.1 Database

3.1.1 Observations

Environment Canada is responsible for collection and distribution of weather data in Canada. The Environment Canada's hourly database mostly consists of rainfall data; the hourly gauges often freeze during winter and estimates obtained from them are not accurate; hence for this part of the study, precipitation could not be used. Hourly rainfall data covering stations around London for the period of 1965-2003 (Figure 1) has been extracted from the Data Access Integration Network (DAI, 2009).
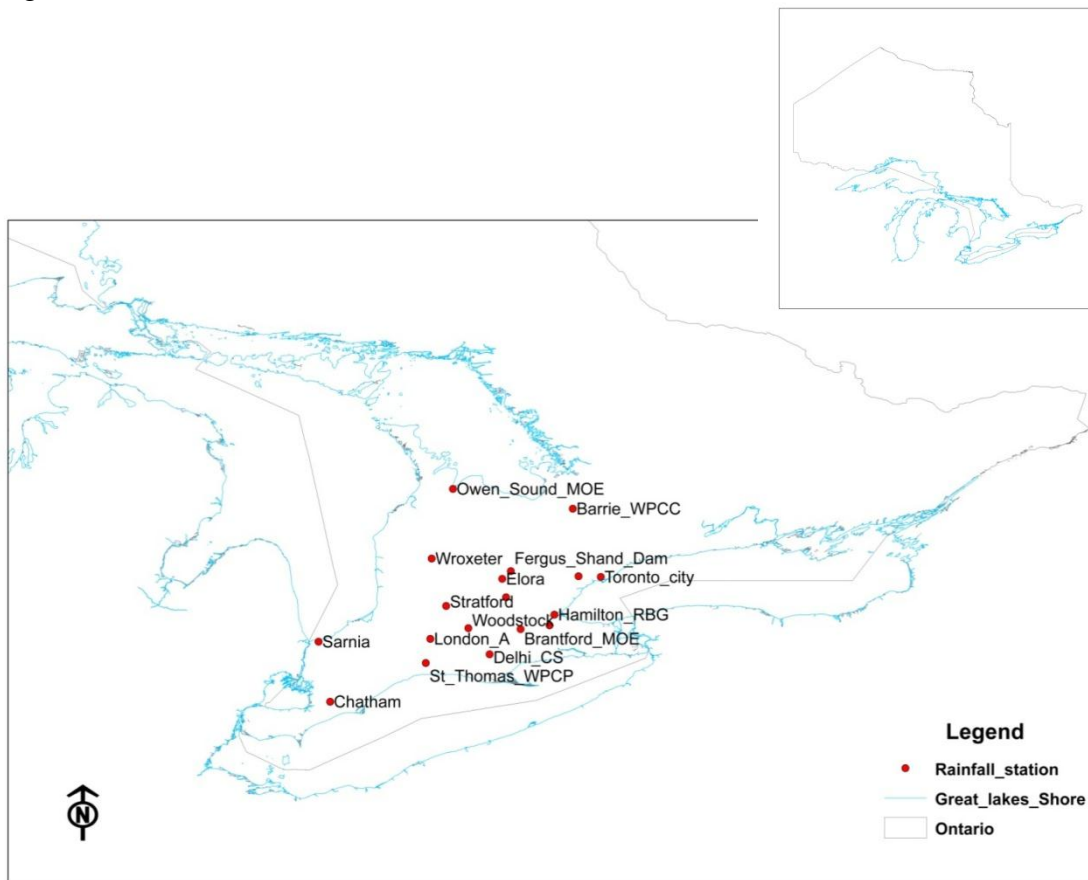
Figure 1: Meteorological Stations Used in the Study

Daily rainfall data for the same stations and same time period is obtained from Environment Canada's Weather Office (http://climate.weatheroffice.ec.gc.ca/climateData/canada_e.html).

The station selection process is highly dependent on the availability of hourly data with adequate lengths. This is an important step in running nearest neighbor based weather generator used in the present study. The number of stations used in the K-NN algorithm influences computation of regional means and the Mahalanobis distance (see section 3.2.1 for details), which affects the choice of nearest neighbor. Data of shorter durations are available only for a handful of stations. So stations closer to London but with shorter record have not been considered in this study. At first, all hourly stations within 200 km radius of London are considered. Next, stations with data going back to 1965 with a record till 2001 are selected. Figure 1 and Table 1 present the details of stations used initially for IDF analysis.

Table 1: Rain Gauge Station Details

Climate ID	Station Name	Latitude (deg)	Longitude (deg)	Elevation (m)	Distance from London (km)
6110557	Barrie WPCC	44.3758	-79.6897	221	190
6140954	Brantford MOE	43.1333	-80.2333	196	75
6131415/6	Chatham WPCP	42.39	-82.2153	180	113
6131982/3	Delhi	42.8667	-80.55	232	52
6142285/6	Elora	43.65	-80.4167	376	91
6142400	Fergus	43.7347	-80.3303	418	102
6153194	Hamilton A	43.1717	-79.9342	238	100
6153300/1	Hamilton RBG	43.2833	-79.8833	102	106
6144475/8	London Int'l A	43.0331	-81.1511	278	0
6116132	Owen Sound MOE	44.5833	-80.9333	179	173
6127519	Sarnia	43	-82.3	181	93
6137361/2	St. Thomas	42.7833	-81.1667	236	28
6148105	Stratford MOE	43.3689	-81.0047	345	39
6158350	Toronto	43.6667	-79.4	113	158
6158733	Toronto Int'l A	43.6772	-79.6306	173	142
6149387	Waterloo A	43.45	-80.3833	317	78
6119500	Wiarton A	44.7458	-81.1072	222	190
6149625	Woodstock	43.1361	-80.7706	282	33

3.1.2 Climate Change Scenarios

Atmosphere-Ocean Global Climate Models (AOGCMs) represent physical processes in the atmosphere, ocean, cryosphere and land surface and are the most advanced tools available for simulating the response of the global climate system to increasing greenhouse gas concentrations. While simpler models have also been used to provide global or regional average estimates of the climate response, only AOGCMs, possibly in conjunction with nested regional models, have the potential to provide geographically and physically consistent estimates of regional climate change needed for climate change impact studies (IPCC, 2007). It is important to note that AOGCMs offer only possibilities of future climate pattern in differing socio-economic conditions depending on continual growth of population, increased carbon dioxide emission, rate of urbanization, etc. Outputs from AOGCMs, thus, should not be considered as the forecasts of future climate conditions.

The Canadian Climate Change Scenarios Network (CCCSN) provides access to several AOGCM models and emission scenarios. The website allows the user to specify the range of geographical co-ordinates required, as well as the climatic variable and time period of interest. For the purpose of this study, precipitation data for two time slices: 1960-1990 (baseline) and 2071-2100 (2080s) are collected. It is important to note here that the AOGCMs provide only precipitation data which is a combination of snow and rainfall during winter. They do not count for rainfall change information. Hence for this study, change in the precipitation between different AOGCM scenarios and historical observed precipitation are used to calculate the change fields and are applied to develop modified rainfall series to be used in the weather generator.

A total of 27 scenarios from 11 AOGCMs, each with two to three emission scenarios (Nakicenovic et al, 2000) are selected for developing future scenarios. Full descriptions of the emissions scenarios and AOGCMs can be found in Appendices B and C. Table 2 provides a complete list of the details of the AOGCM scenarios used in this study.

Table 2: List of AOGCM Models and Emission Scenarios

GCM models	Sponsors, Country	SRES scenarios	Atmospheric resolution	
			Lat	Long
CGCM3T47, 2005	Canadian Centre for Climate Modelling and Analysis, Canada	A1B, A2, B1	3.75°	3.75°
CGCM3T63, 2005		A1B, A2, B1	2.81°	2.81°
CSIROMK3.5, 2001	Commonwealth Scientific and Industrial Research Organization (CISRO) Atmospheric Research, Australia	A1B, A2, B1	1.875°	1.875°
ECHAM5AOM, 2005	Max Planck Institute for Meteorology, Germany	A1B, B1, A2	1.875°	1.875°
ECHO-G, 1999	Meteorological Institute of the University of Bonn, Meteorological Research Institute of the Korea Meteorological Administration (KMA), and Model and Data Group, Germany/Korea	A1B, B1, A2	3.9°	3.9°
GFDLCM2.1, 2005	U.S. Department of Commerce/ National Oceanic and Atmospheric Administration (NOAA)/Geophysical Fluid Dynamics Laboratory (GFDL), USA	A1B, B1, A2	2°	2.5°
GISSAOM, 2004	National Aeronautics and Space Administration (NASA)/ Goddard Institute for Space Studies (GISS), USA	A1B, B1	3°	4°
MIROC3.2HIRES, 2004	Centre for Climate System Research (University of Tokyo), National Institute for Environmental Studies, and Frontier Research Centre for Global Change (JAMSTEC), Japan	A1B, B1	1.125°	1.125°
MIROC3.2MEDRES, 2004		A1B, A2, B1	2.8°	2.8°
CCSR/NIES B21, 1999	Centre for Climate System Research, University of Tokyo and National Institute for Environmental Studies, Japan	B21	5.6°	5.6°
CSIROMK2b, 1997	Commonwealth Scientific and Industrial Research Organization (CISRO) Atmospheric Research, Australia	B11	5.6°	3.2°

3.2 Development of Methodology

Figure 2 presents the schematic of the methods adopted for generating IDF curves for 2080s incorporating uncertainties from AOGCM scenario. The step by step procedures are presented below.

3.2.1 Downscaling

Stochastic weather generators simulate weather data to assist in the formulation of water resource management policies. The basic assumption for producing synthetic sequences is that the past would be representative of the future. They are essentially complex random number generators, which can be used to produce a synthetic series of data. This allows the researcher to account for natural variability when predicting the effects of climate change.

In order to reduce multi-dimensionality and collinearity associated with the large number of input variables, principal component analysis has been integrated with the weather generator. The process requires selecting appropriate principal components (PCs) that will adequately represent most information of the original dataset.

The WG-PCA algorithm with p variables and q stations works through the following steps:

1) Regional means of p variables for all q stations are calculated for each day of the observed data:

$$\overline{X_t} = \lfloor \overline{x}_{1,t}, \overline{x}_{2,t}, ..., \overline{x}_{p,t} \rfloor \quad \forall t = \{1,2,...,T\} \tag{3.1}$$

Flowchart

Left column (top to bottom):

- Observed Rainfall (Daily)
- → Station Selection / Cross-Correlation Analysis, Regression Analysis
- Selected Observed Rainfall (Daily)
- → (Unperturbed)
- Simulated Output (Present)
- Simulated Hourly Output (Present)
- Maximum Rainfall for Different Durations (Present)
- IDF Curve for Present

Center:

- Weather Generator (decision)
- Disaggregation
- AMS

Right column (top to bottom):

- Gridded AOGCM Outputs (27 Scenarios)
- → Linear Interpolation
- AOGCM Outputs on Station Scale
- → Change Field Analysis
- Modified Daily Output (27 Scenarios)
- Daily Outputs 2080s (27 Scenarios)
- Hourly Output 2080s (27 Scenarios)
- Max. Rainfall for Diff. Durations 2080s (27 Scenarios)
- IDF Curves for 2080s (27 Scenarios)
- → Quantifying Uncertainty / Plug-in Kernel
- IDF Curve 2080s (Resultant Scenario)

Weather Generator → (Perturbed) → Daily Outputs 2080s (27 Scenarios)

Figure 2: Schematic Diagram of Developing IDF Curve

$$\text{where } \bar{x}_{i,t} = \frac{1}{q}\sum_{j=1}^{q} x_{i,t}^{j} \quad \forall i = \{1, 2, ..., p\} \tag{3.2}$$

2) Selection of potential neighbors, L days long where $L=(w+1) \times (N\text{-}1)$ for each of p individual variable with N years of historic record, and a temporal window of size w which can be set by the user of the weather generator. The days within the given window are all potential neighbors to the feature vector. N data which correspond to the current day are deleted from the potential neighbors so the value of the current day is not repeated.

3) Regional means of the potential neighbors are calculated for each day at all q stations.

4) A covariance matrix, C_t of size $L \times p$ is computed for day t.

5) The first time step value is randomly selected for each of p variables from all current day values in the historic record.

6) Next, using the variance explained by the principal component, Mahalanobis distance is calculated with equation 3.

$$d_k = \sqrt{(PC_t - PC_k)^2 / Var(PC)} \quad \forall k = \{1,2,...,K\} \tag{3.3}$$

Where PC_t is the value of the current day and PC_k is the nearest neighbor transferred by the Eigen vector. The variance of the first principle component is $Var(PC)$ for all K nearest neighbors.

7) The selection of the number of nearest neighbors, K, out of L potential values using $K = \sqrt{L}$.

8) The Mahalanobis distance d_k is put in order of smallest to largest, and the first K neighbors in the sorted list are selected (the K Nearest Neighbors). A discrete probability distribution is used which weights closer neighbors highest in order to resample out of the set of K neighbors. Using equations 4 and 5, the weights, w, are calculated for each k neighbor.

$$w_k = \frac{1/k}{\sum\limits_{i=1}^{K} 1/i} \qquad \forall k = \{1,2,...,K\} \tag{3.4}$$

Cumulative probabilities, p_j, are given by:

$$p_j = \sum_{i=1}^{j} w_i \tag{3.5}$$

9) A random number u (0,1) is generated and compared to the cumulative probability calculated above in order to select the current day's nearest neighbor. If $p_1 < u < p_k$, then day j for which u is closest to p_j is selected. However, if $p_i > u$, then the day which corresponds to $d1$ is chosen. If $u=p_K$, then the day which corresponds to day d_K is selected. Upon selecting the nearest neighbor, the K-NN algorithm chooses the weather of the selected day for all stations in order to preserve spatial correlation in the data (Eum et al, 2009).

10) In order to generate values outside the observed range, perturbation is used. A conditional standard deviation σ for K nearest neighbors is estimated. For choosing the optimal bandwidth of a Gaussian distribution function that minimizes the asymptotic mean integrated square error (AMISE), Sharma et al. (1997) reduced Silverman's (Silverman 1986, pp. 86-87) equation of optimal bandwidth into the following form for a univariate case:

$$\lambda = 1.06\sigma K^{-1/5} \tag{3.6}$$

Using the mean value of the weather variable $x_{i,t}^j$ obtained in step 9 and variance $(\lambda\sigma_i^j)^2$, a new value $y_{i,t}^j$ can be achieved through perturbation (Sharma et al. 1997).

$$y_{i,t}^j = x_{i,t}^j + \lambda\sigma_i^j z_t \tag{3.7}$$

Where z_t is a random variable, distributed normally (zero mean, unit variance) for day t. Negative values are prevented from being produced for precipitation by employing a largest acceptable bandwidth: $\lambda_a = x^j_{*_t}/1.55\sigma^j_*$ where * refers to precipitation. If again a negative value is returned, a new value for z_t is generated (Sharif and Burn, 2006).

3.2.2 Bias Correction of Downscaled Outputs

The downscaling process scales down coarse grid outputs of AOGCMs into the scale of interest. However, significant simulation bias still may exist from the initializations of atmospheric-oceanic processes. Hence, employing coarse resolution global model output for regional and local climate studies requires an additional bias correction step based on the ability of the AOGCMs to reproduce the past climate. In this study, bias from the downscaled outputs is corrected by the following equation:

Bias in AOGCM,

$$b_i = \frac{x_i - y_i}{x_i} * 100 \tag{3.8}$$

Where,

b_i = bias from different AOGCMs

x_i = Monthly mean of observed precipitation for 1965-1990

y_i = Monthly mean from different AOGCMs for 1965-1990

the correction factor for the AOGCMs is then calculated using,

$$c_i = \frac{b_i}{100} + 1 \tag{3.9}$$

So, the treated downscaled rainfall for 2080s,

$$p_j = c_i * p_i \tag{3.10}$$

where,

p_i = untreated daily downscaled rainfall for 2080s

3.2.3 Disaggregation

The disaggregation scheme works by extracting rainfall event records from the hourly observed data. A rainfall event can be defined as a period of non-zero rainfall for two or more days where the total amount of rainfall during the consecutive days is considered as the event rainfall value. Once the rainfall events are extracted from the historic record, they are disaggregated by a K-nearest neighbor approach. The algorithm considers daily rainfall produced by the weather generator for day t, for each station. A set of potential events are selected from the observed record from which once such event is chosen based on which the daily output is disaggregated into hourly values.

The selection of neighboring events from the observed record follows simple rule:

Only events within a moving window of w_h days are selected to account for the seasonally varied temporal distribution of rainfall. Events are selected from the prescribed moving window from all years in the historic record of events as a potential set of neighbors. The daily totals from downscaled outputs are compared with the set of neighboring event totals to assure that the only disaggregation of similar events is considered.

Observed hourly data is used as a template on how the hourly values of the generated outputs would look like. A specific number of days are considered to compare with the present day value. The best match is determined by (Mansour and Burn, 2010):

$$z_i = \sqrt{(w_1 * (y_i - x_i)^2) + (w_2 * (e_y - e_x)^2)} \quad (3.11)$$

Where, y_i is the daily rainfall output from weather generator, x_i is the historical observed daily rainfall, e_x and e_y are the events calculated from WG outputs and historical observed data respectively. The weights w_1, w_2 are used to identify the best historical hourly ratio of the data. An hourly value set within the moving window of days can be chosen for a similar event w_2 or for the daily total rainfall w_1. The combination of the weights, which provide the lowest z_i for each value within the window, is considered as the daily ratio of historical hourly values used to disaggregate the WG's daily data into hourly values. The ratio of the hourly values found within the chosen day is applied to the daily value to create a plausible hourly set-up for the given daily data. This is done based on the methods of fragments (Svanidze, 1977; Sharif et al., 2007). The fragments represent the fraction of daily rainfall that occur during each hour of the day summing to unity and can be expressed as:

$$f_i = \frac{h_i}{\sum_{i=1}^{n} h_i} \qquad (3.12)$$

where f_i represents the fragments calculated for hour i, h_i is the chosen hourly data from observations, n is the number of hours in a day which is 24. The fragments are then multiplied with the daily data to produce data for each hour:

$$h_i' = f_i \times d \qquad (3.13)$$

where d is the daily rainfall (mm). This program has been sent daily data that already had known hourly values and the results have been compared in an attempt to verify that the model works correctly.

28

This approach utilizes locally observed data using a non-parametric method avoiding the chance of errors that may occur from the parametric methods due to theoretical distribution fits, parameter estimations and calibration. Additionally, there is high likelihood that the statistical characteristics of the disggregated rainfall are stored by applying the resampling algorithm.

3.2.4 Generation of Rainfall for Different Durations

Sampling of rainfall data for estimating rainfall extremes are commonly proceeded using two approaches: the annual maxima series (AMS) or block maxima and peak over threshold (POT) or partial duration series (PDS) (Coles, 2001). Literatures have identified limitations and advantages of both methods. Madsen et al. (1997), Buishand et al. (1990), Rasmussen et al. (1994) found POT to be a better approach than AMS. While Kartz et al. (2002), Smith (2003), de Michele and Salvadori (2005) suggested use of both methods. By definition, AMS approach includes the yearly peaks in the observational period while the POT involves all the peak events that exceed a given threshold value. The AMS method is more straightforward. If the number of annual maxima is small (<100), the obtained estimates may be sensitive to outliers. It is an asymptotic method that works well if the number of inputs from which a maximum is considered, is large. Jeruskova et al., 2006 showed that convergence to limit any distribution fit can be slow. For determining annual maxima, the maxima of 365 daily values are considered. The seasonal effect may also play a role. Application of POT is somewhat difficult than the AMS because of it's selection of an appropriate threshold. For a satisfactory stability of the obtained results, testing of several threshold values such as 90%, 95% and 98% are recommended. Jeruskova et al. (2006) have shown that the POT method may work well for short memory series only. For longer data series, the series should be split into several more homogeneous groups. Both methods however, have their own disadvantages too; the AMS may

neglect certain high values, while the POT may suffer from serial correlation problem (Jervis et al., 1936; Langbein, 1949;, Taesombat and Yevjevich, 1978).

3.2.5 Intensity-Duration-Frequency Analysis

Rainfall intensity-duration-frequency (IDF) curves are derived from the statistical analysis of rainfall events over a period over time and used to capture important characteristics of point rainfall for shorter durations. It is considered as a convenient tool for gathering regional rainfall information required for municipal storm water management works. Site specific curves represent intensity-time relationship for a specific return period from a series of storms. Information is summarized by plotting the durations on the horizontal axis, the rate of rainfall (intensity in depth per unit of time) on the vertical axis and the curves for each design storm return period. Frequency is expressed in terms of return period, T, the average length of time between rainfall events that equals or exceed any given magnitude. For each selected duration, annual maximum rainfall is extracted from the rainfall data and frequency analysis is performed to the annual maximum rainfall to fit a probability distribution for standardizing the characteristics of rainfall for each station with varying rainfall record.

In Canada, Environment Canada is responsible (a) for collection and quality control of rainfall data and (b) for providing the rainfall extreme information in the form of IDF curves. Gumbel's Extreme Value distribution is normally used to fit the annual extremes of rainfall using AMS method. It is acknowledged here that due to changes in future precipitation extremes, the future rainfall may not follow the conventionally used Gumbel's distribution. It would be adequate to consider a generalized extreme value (GEV) distribution. But the inherent uncertainties in the responses of AOGCM outputs do not guarantee GEV as the best fit for all AOGCMs. Furthermore, fitting of three parameters for the GEV distribution by maximum

likelihood method requires considerable computation time, and will be different for different AOGCM responses. For simplification, and to comply with Environment Canada's procedure, use of Extreme Value (EV) type 1 which is Gumbel distribution is adopted in this study. The Gumbel probability distribution is expressed (Watt et al., 1989):

$$x_t = \mu_z + K_T\,\sigma_z \tag{3.14}$$

where x_t represents the magnitude of the T year event, μ_z and σ_z are the mean and standard deviation of the annual maximum series, and K_T is a frequency factor depending on the return period, T. The frequency factor K_T is obtained using the following equation:

$$K_T = \frac{-\sqrt{6}}{\pi}[0.5772 + \ln(\ln(\frac{T}{T+1}))] \tag{3.15}$$

Meteorological Service of Canada (MSC) uses the above method to calculate rainfall frequency for durations of 5, 10, 30 minutes and 1, 2, 6. 12, 24 hours. Since most of the stations do not have observed sub-hourly data, the calculation of the frequencies for periods shorter than 1 hour may be based on the ratios provided by the World Meteorological Organization (MTO, 1997):

Duration (min)	5	10	15	30
Ratio (n-min to 60-min)	0.29	0.45	0.57	0.79

However, for the present study, durations shorter than 1 hour are not considered.

The IDF data is next fitted to a continuous function in order to make the process of IDF data interpolation more efficient i.e. if the ratio of any duration is not available, the IDF data is fitted to the following three parameter function:

$$i = \frac{A}{(t_d + B)^C} \tag{3.16}$$

where i presents the rainfall intensity in mm/hr, t_d is the duration of rainfall in minute, $A, B, and\ C$ are the constants. To obtain optimal values for these three parameters, a reasonable value of B is assumed and the values of $A\ and\ C$ are estimated by the least square method. The process is repeated to achieve the closest fit of the data (MTO, 1997). Plots of rainfall intensity vs. duration for each return period is then produced from the fitted IDF data to equation 3.14.

3.2.6 Uncertainty Quantification

A practical approach to deal with AOGCM and scenario uncertainties originating from inadequate information and incomplete knowledge should: (i) be robust with respect to model choice; (ii) be statistically consistent in a uniform application across different spatial scales such as global, regional or local/watershed scales; (iii) be flexible enough to deal with the variety of data; (iv) obtain the maximum information from the sample; and (v) lead to consistent results. Most parametric methods do not meet all these requirements.

Probability Density Function (PDF) is commonly used to describe the nature of data. In applications an estimate of the unknown $PDF = f(\ )$ based on random sample $x_1, x_2, \ldots \ldots x_n$ from $f(\ )$ is calculate in the form of $\widehat{PDF} = \hat{f}(\ )$. Probability distribution functions estimated by any nonparametric method without prior assumptions can be suitable to quantify AOGCM and scenario uncertainties. Several approaches such as kernel methods, orthogonal series methods,

penalized-likelihood methods, k-nearest neighbor methods, Bayesian-spline methods, and maximum-likelihood or histogram like methods can be found in the literature (Adamowski, 1985).

Kernel density estimation method has been widely used as a viable and flexible alternative to parametric methods in hydrology (Sharma et al., 1997; Lall, 1995), flood frequency analysis (Lall et al., 1993; Adamowski, 1985), and precipitation resampling (Lall et al., 1996) for estimating probability density function.

A kernel density estimate is formed through the convolution of kernels or weight functions centered at the empirical frequency distribution of the data. A kernel density estimator involves the use of kernel function (K(x)) defined by:

$$\int_{-\infty}^{\infty} K(x)dx = 1 \tag{3.17}$$

A PDF thus, can be used as a kernel function. The Parzen-Rosenbalt kernel density estimate $f_n(x)$ at x, from a sample of $\{x_1, \ldots, x_i, \ldots, x_n\}$ of sample size n can is given by:

$$\widehat{f}_h(x) = \frac{1}{n}\sum_{i=1}^{n}\frac{1}{h}K_h\left(\frac{x-x_i}{h}\right) \tag{3.18}$$

where $t = \left(\frac{x-x_i}{h}\right)$ and $k_h(t)$ is a weight or kernel function required to satisfy criteria such as symmetry, finite variance, and integrates to unity. Successful application of any kernel density estimation depends more on the choice of the smoothing parameter or bandwidth *(h)* and the type of kernel function *K(.)*, to a lesser extent. Bandwidth for kernel estimation may be evaluated by minimizing the deviation of the estimated PDF from the actual one.

The behavior of the estimator (equation 3.18) may be analyzed mathematically under the assumption that the data sets represent independent realizations from a probability density $f(x)$. The basic methodology of the theoretical treatment is to discuss the closeness of estimator $\hat{f}$ to the true density, f. Successful application of the estimator depends mostly on the choice of a kernel and a smoothing parameter or bandwidth. Literatures have found that the choice of bandwidth is more critical. A change in kernel bandwidth can dramatically change the shape of the kernel estimate (Efromovich, 1999). For each x, $\hat{f}(x)$ can be thought as a random variable because of it's dependence on $X_1, X_2, \dots \dots X_n$. Except otherwise stated, $\sum$ will refer to a sum for $i = 1 \ to \ n$ and $\int$ to an integral over the range $(-\infty, \infty)$.

The discrepancy of the density estimator $\hat{f}$ from it's true density f can be measured by mean square error (MSE):

$$MSE_x(\hat{f}) = E[(\hat{f}(x) - f(x)]^2 \tag{3.19}$$

By standard elementary properties of mean and variance,

$$MSE_x(\hat{f}) = \{E[(\hat{f}(x) - f(x)]^2\} + var \ \hat{f}(x), \tag{3.20}$$

the sum of the squared bias and the variance at x. In many applications a trade-off is applied between the bias and the variance in equation (3.20); the bias can be reduced by increasing the variance and vice versa by adjusting the degree of smoothing.

It can be obtained by minimizing the mean integrated square error (MISE), a widely used measure of global accuracy of $\hat{f}$ as an estimator of f (Rosenblatt, 1956; Adamowski, 1985; Scott et al., 1981, Jones et al., 1996) defined as:

$$MISE\left(\hat{f}\right) = E \int [(\hat{f}(x) - f(x)]^2 dx \qquad (3.21)$$

or in alternative forms,

$$MISE(\hat{f}) = \int MSE_x(\hat{f})dx$$

$$= E \int [(\hat{f}(x) - f(x)]^2 dx + \int var\,(\hat{f})dx \qquad (3.22)$$

which gives the $MISE$ as the sum of the integrated square bias and the integrated variance.

Asymptotic analysis provides a simple way of quantifying how the bandwidth h works as a smoothing parameter. Under standard assumptions, MISE is approximated by the asymptotic mean integrated square error (AIMSE) (Jones et al., 1996):

$$AMISE(h) = n^{-1}h^{-1}R(K) + h^4 R(f^{"})\left(\int x^2 \,{}^{K}\!/_{2}\right)^2 \qquad (3.23)$$

where $R(\varphi) = \int \varphi^2(x)dx$ and $\int x^2\,K = \int x^2\,K(x)dx$, n is sample size, h is bandwidth. The first term (integrated variance) is large when h is too small, and the second term (integrated squared bias) is large when h is too large.

The minimizer of $AIMSE(h)$ is easily calculated as:

$$AMISE(h) = \left[\frac{R(k)}{nR(f^{"})(\int x^2 K)^2}\right]^{1/5} \qquad (3.24)$$

In this study the solve-the-equation-plug-in approach is used to derive the data-driven bandwidth for estimating the densities.

The main thought behind the 'solve the equation plug in' approach is to plug an estimate of the unknown $R(f^{"})$ in the equation (3.24). The major challenge is to estimate a pilot bandwidth.

The 'solve the equation' approach proposed by Hall (1980), Sheather (1983, 1986) and later refined by Sheather and Jones (1991) is used in this study. The smallest bandwidth, h_{SJPI} is considered as the solution of the fixed point equation

$$h = \left[\frac{R(K)}{nR\left(\hat{f}''_{g(h)}\right)(\int x^2 K)^2} \right]^{\frac{1}{5}} \tag{3.25}$$

A dummy minimizer in the form $g(h)$ is used to provide better representation of $R(f'')$. It is done by estimating an analogue of h_{AMISE} for estimating $R(f'')$ by $R\left(\hat{f}''_g\right)$.

The minimizer of the asymptotic mean square error (AMSE) is expressed as:

$$g_{AMSE} = C_1\{R(f''')\}C_2(K)n^{\frac{-1}{7}} \tag{3.26}$$

for suitable functional C_1 and C_2. The expression of g in terms of h comes from solving the representation of h_{AIMSE} for n and substituting to get

$$g(h) = C_3\{R(f''), R(f''')\}C_4(K)h^{5/7} \tag{3.27}$$

for appropriate functionals C_3, C_4. The unknowns $R(f'')$ and $R(f''')$ are estimated by $R(\hat{f}'')$ and $R(\hat{f}''')$, with bandwidths chosen by reference to a parametric family, as for h_{ROT}.

Many variations have been tested for treatment of $R(\hat{f}'')$ and $R(\hat{f}''')$. The major contribution has been to try to reduce the influence of the normal parametric family even further by using pilot kernel estimates instead of normal interference (Jones et al., 1996). Park and Marron (1990) has shown the improvements in terms of the asymptotic rate of convergence up to a certain point.

4. Results and Discussion

This chapter presents the results of the methodology introduced above for the development of IDF curve for 2080s. Results are presented for the City of London.

4.1 Selection of Appropriate Stations

The number of stations used to generated long sequence of rainfall series influence outputs of weather generator. Stations surrounding the point of interest help to capture the spatial and temporal characteristics in the region. In cases where only limited data is available, surrounding stations may help to add spatial and temporal characteristics of the rainfall values. Conversely, use of too many stations can be computationally expensive and unnecessary; especially for short duration rainfall where convective storms are highly localized weather patterns, operating on relatively small spatial scales. Stations located too far may affect the performance of weather generator. So regression and cross correlation analysis are performed for identifying important stations for London. For regression analysis, the stations are grouped based on selected distances from London (Table 3). Regression results for each group are provided in the Appendix A. The results are expressed in terms of t-test statistics, p values and the coefficient of determination.

Results from the Appendix A show significant t-test statistic for all predictors reducing the possibility of over-fitting by an insignificant predictor. The term 'probability value' (p) denotes the results of the testing of hypothesis that the regression coefficient is equal to zero which in turn quantifies the importance of the regressor. A result of α in the probability value column for a predictor X denotes that with $(100) \times (1-\alpha)\%$ of confidence one can reject the hypothesis that

the coefficient of predictor X is zero. Low or near zero value of α is desirable as it is inversely related to the importance of a predictor.

Table 3: Groups for Regression Analysis based on Distances

Stations	Groups based on distances (km)						
	0-200	0-175	0-150	0-125	0-100	0-75	0-50
Barrie WPCC	√						
Brantford MOE	√	√	√	√	√	√	
Chatham WPCP	√	√	√	√			
Delhi	√	√	√	√	√	√	
Elora	√	√	√	√	√		
Fergus	√	√	√	√			
Hamilton A	√	√	√	√	√		
Hamilton RBG	√	√	√	√			
London Int'l A	√	√	√	√	√	√	√
Owen Sound MOE	√	√					
Sarnia	√	√	√	√	√		
St. Thomas WPCP	√	√	√	√	√	√	√
Stratford MOE	√	√	√	√	√	√	√
Toronto	√	√					
Toronto Int'l A	√	√	√				
Waterloo A	√	√	√	√	√		
Wiarton A	√						
Woodstock	√	√	√	√	√	√	√
Total	**18**	**16**	**14**	**13**	**10**	**6**	**4**

The t-statistics for the independent variables are equal to their coefficient estimates divided by their respective standard errors. In theory, the t-statistic of any one variable may be used to test the hypothesis that the true value of the coefficient is zero (which is to say, the variable should not be included in the model). In a standard normal distribution, only 5% of the values fall outside the range plus-or-minus 2 A low t-statistic (or equivalently, a moderate-to-large exceedance probability) for a variable suggests that the SEE would not be adversely affected by its removal. The rule-of-thumb in this regard is to remove the least important variable if its t-statistic is less than 2 in absolute value, and/or the exceedance probability is greater than .05

(Minitab help, 2009). From the results it is seen that stations within 100 km distances appear to be the best option for London. This can be clearly seen from the coefficient of determination plot in Figure 3 where addition of more stations, beyond 100 km distance apparently cannot improve the model performance.
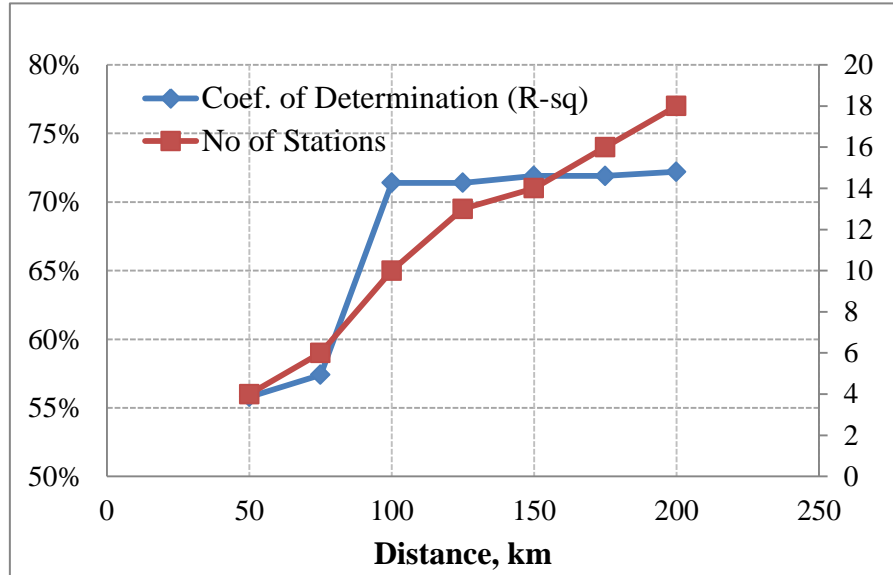
Figure 3: Performances of Stations based on Distance

Next, the cross correlation analysis is performed to identify the correlation between the stations (Table 4). Results show that stations within 100 km radius are correlated well, with correlation greater than 60% for all stations but Elora. However, the regression test shows that inclusion of Elora may provide important information to the spatial and temporal pattern of London. So it is included for IDF analysis. So finally, nine stations with hourly and daily rainfall data from 1965-2001, located within 100 km radius of London station have been selected for further analysis.

Both historical daily and hourly data contains missing values. Inverse distance weighted methods is applied to fill the missing values.

Table 4: Cross-Correlation Results for Stations Within 200 km Distance from London

Stations	Distance (km)	Lag				
		-2	-1	0	1	2
London A	0	-0.004	0.094	1.000	0.094	-0.004
Waterloo A	78	-0.004	0.063	0.729	0.097	0.000
Woodstock	33	0.003	0.273	0.723	0.022	-0.012
Sarnia	93	0.018	0.131	0.676	0.054	-0.014
Hamilton A	100	0.003	0.050	0.670	0.136	-0.008
Delhi CS	52	-0.004	0.236	0.657	0.020	-0.014
Brantford MOE	75	0.000	0.249	0.645	0.026	-0.019
Stratford MOE	39	-0.005	0.263	0.633	0.028	-0.004
Hamilton RBG	106	0.002	0.214	0.618	0.037	-0.008
Toronto Int'l A	142	-0.002	0.043	0.610	0.125	0.000
St. Thomas WPCP	28	-0.009	0.344	0.609	0.030	-0.008
Fergus	102	-0.005	0.203	0.564	0.033	-0.009
Toronto	158	-0.005	0.158	0.564	0.028	-0.012
Elora	91	-0.002	0.199	0.550	0.066	0.002
Chatham WPCP	113	-0.006	0.278	0.488	0.008	-0.013
Barrie	190	-0.010	0.122	0.461	0.062	-0.007
Wiarton A	190	-0.021	0.049	0.454	0.101	-0.009
Owen Sound	173	-0.024	0.146	0.373	0.047	-0.005

4.2 Development of Climate Change Scenarios

Climate change scenarios from AOGCM outputs (Table 2) are used to condition the input data using the weather generator. Outputs from AOGCMs for 1961-1990 represent baseline climate against which the future climate change scenarios for 2071-2099 (2080s) have been computed.

Based on the AOGCM data, change fields for each scenario is calculated as the difference between the monthly mean precipitation from their 1961-1990 mean.

This difference is then multiplied with the locally observed station data to generate climate change scenarios appropriate for the City of London at a daily time scale. As an example, if the change field for the month of July and August are 10% and -5%, all daily July and August rainfall values are multiplied by a factor of 1.05 and 0.95, respectively. This newly modified data is then used with the weather generator to generate daily time series of any preferred length for different scenarios. For this study, 27 different climate scenarios are developed which represent different realizations of future. Comparison of 1961-1990 mean historical observed rainfall with those developed from different scenarios for base climate reveal that significant bias still exit in the base climate which is used to initialize the future climate; which means the bias may be carried out in the downscaled output. Table 5 (a) presents a comparison between the monthly mean precipitation from different AOGCM scenarios and historical observed values. Mean monthly precipitation vary significantly for between months for all models.

Table 5 (a): Monthly Mean Precipitation (mm) from Different AOGCMs for 1965-1990

Scenarios/month	Jan	Feb	Mar	Apr	May	Jun	Jul	Aug	Sep	Oct	Nov	Dec
Observed	2.28	2.21	2.51	2.65	2.48	2.80	2.46	2.79	3.04	2.66	3.17	3.16
CGCM3T47	1.99	1.95	2.25	2.71	2.88	2.66	2.12	2.11	2.35	2.29	2.88	2.73
CGCM3T63	2.14	1.80	2.45	2.84	3.69	3.42	3.00	2.40	2.30	2.87	2.67	2.93
CSIROMK3	1.94	2.16	2.44	2.97	3.28	2.64	2.42	1.80	1.72	2.31	2.42	2.21
ECHAM5OM	3.01	3.63	3.62	4.11	4.33	4.41	3.58	3.47	3.32	2.47	2.99	3.09
ECHO-G	2.08	2.10	2.49	3.43	4.45	3.66	3.82	3.18	2.59	2.67	2.92	2.21
GFDLCM2.1	2.46	2.83	2.86	2.90	3.54	3.19	3.23	3.04	3.36	2.29	2.83	2.62
GISSAOM	2.04	2.22	2.51	2.79	2.54	2.21	2.59	2.91	3.18	3.04	2.57	2.56
MIROC3.2_HIRES	2.88	2.56	2.97	3.32	3.01	3.23	3.76	3.34	3.40	2.90	3.28	3.14
MIROC3.2_MEDRES	2.21	2.57	2.64	2.86	2.92	3.49	3.71	3.00	2.96	2.47	2.52	2.40
CCSRNIES_B21	1.84	2.24	2.86	3.25	3.63	4.18	4.77	3.52	2.07	1.40	1.73	2.05
CSIROMk2b_B11	1.51	1.53	1.74	2.34	2.50	3.21	3.26	2.20	1.71	1.88	1.79	1.64

4.3 Verification of the IDF Generation Methods

Once preparation of data is complete, daily weather generator described in section 3.2.1 is

used to simulate a sequence of rainfall for all stations. For the verification purpose, the perturbation of the weather generator described in section 3.3.1 is kept off in order to replicate the exact scenario as the historical, observed, one.

This study uses 10 stations for the period of 1965-2003 (N=39) to simulate different rainfall scenarios. Employing the temporal window of 14 days (w=14) and 39 years of historic data (N=39), 584 days are considered as potential neighbors *(L=(w+1) x N-1=584)*. Each case is simulated three times thus generating 117 years of simulated output. It is expected that such length of output is sufficient enough to estimate event with return period of 100 years.

In order to test the output of the weather generator, the box and whisker plots for monthly historical simulated rainfall are created (Figure 4).
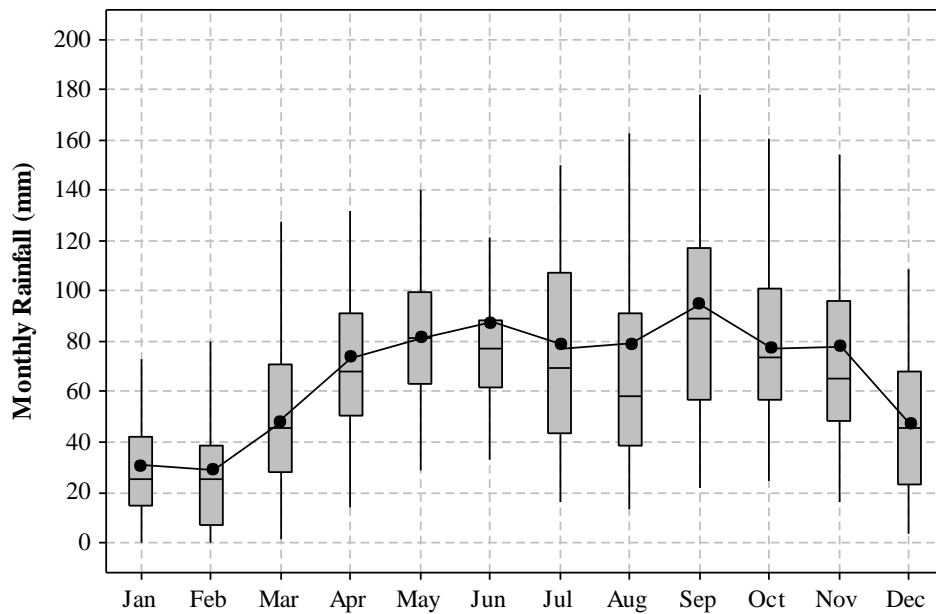
Figure 4: Box and Whiskers Plot of Simulated Monthly Rainfall in London

The boxes show the 25th percentile, 50 percentile and 75th percentiles of data while the whiskers, plotted with 1.5 times the inter-quartile range from the boxes. For all cases historic

observed means are shown in terms of line plot to assess the ability of the weather generator to reproduce the temporal and spatial character of rainfall for the City of London. From the Figure 4, it is seen that the model has been able to replicate the historic observed pattern adequately.

Next, the daily rainfall is disaggregated into hourly values using the method described in section 3.2.3. The comparison of the performance of the historic simulated hourly values with the observed hourly data is presented in terms of frequency plots (Figure 5).
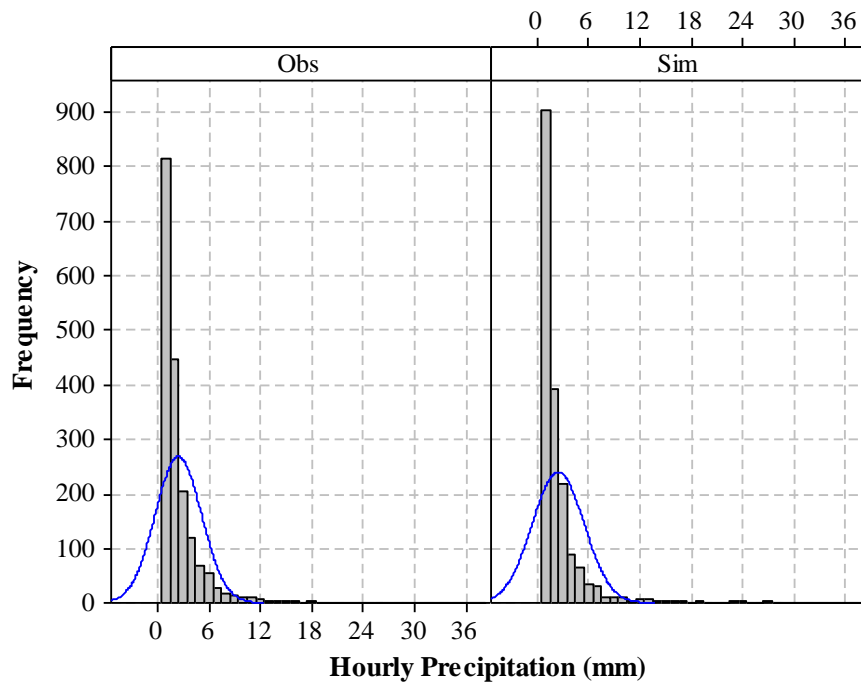
Figure 5: Frequency Plots of Observed (Obs) and Simulated (Sim) Hourly Rainfall

The frequency of small range rainfall is slightly over-estimated and the mid range rainfall is slightly under-estimated by the disaggregation model. Overall, the frequency of the extreme rainfall is captured well.

Finally, the annual maximum rainfall for 1, 2, 6, 12 and 24 hour durations is generated to fit Gumbel distribution for calculating return periods. These are then compared with the IDF information obtained from Environment Canada (EC) (Table 6). It should be noted that the

Environment Canada uses rainfall data from 1943-2001 to develop IDF curves for London. However, hourly data is available only from 1961; data prior to 1961 may exist in paper form and are not available. For the present study, the hourly rainfall data for London is further reduced down to 1965 for matching rainfall data from other nearby stations to be used for multi-site weather generator.

Table 6 (a): Comparison of Extreme Rainfall in London in terms of Depth (mm)

Historic Unperturbed (1965-2003)	Return Period, T years					
Duration, hrs	2	5	10	25	50	100
1	21.80	30.38	36.06	43.24	48.56	53.85
2	28.05	40.11	48.09	58.18	65.66	73.09
6	36.41	49.90	58.83	70.11	78.49	86.80
12	42.61	56.33	65.41	76.89	85.40	93.86
24	49.70	64.63	74.52	87.01	96.28	105.48
EC (1943-2003)	Return Period, T years					
Duration, hrs	2	5	10	25	50	100
1	24.40	35.30	42.50	51.60	58.30	65.00
2	29.60	41.60	49.50	59.60	67.00	74.40
6	36.70	48.20	55.80	65.40	72.50	79.60
12	43.00	54.70	62.50	72.40	79.70	87.00
24	51.30	66.80	77.10	90.00	99.60	109.20

Table 6 (a) presents the intensity-duration-frequency data obtained from the historic unperturbed scenario together with the IDF data generated by EC. The results obtained are compared in terms of the relative differences using the following relationship:

$$Relative\ difference = \frac{|x_1 - x_2|}{\frac{x_1 + x_2}{2}} \times 100 \qquad (3.28)$$

Table 6 (b) presents the relative difference of rainfall intensity between the historic unperturbed and the EC data. The short duration rainfall (1 hr) is underestimated by the historic unperturbed scenario, while the intermediate (2, 6, 12 hrs) and longer (24 hrs) duration rainfalls are able to closely replicate the EC generated intensities for all return periods. Overall, the performance of the historic unperturbed scenario is satisfactory.

Table 6 (b): Relative Difference between EC IDF Information and Historic Unperturbed Scenario

Duration, min	Return Period, years					
	2	5	10	25	50	100
60	11.25	14.98	16.39	17.63	18.22	18.76
120	5.38	3.66	2.89	2.42	2.02	1.78
360	0.80	3.46	5.29	6.96	7.93	8.65
720	0.91	2.94	4.56	6.02	6.91	7.58
1440	3.18	3.30	3.40	3.37	3.39	3.46

4.4 IDF Results for Future Climate

The perturbation process inside the weather generator is added (described in section 3.2.1) to generate IDF information using the historical observed rainfall. This scenario called 'historical perturbed' assumes that the future climate will continue to change as the consequence of already altered green house gas concentrations in the atmosphere, ignoring any future change in green house gas emissions.

The daily weather generator output, after being disaggregated into hourly rainfall, is next used to generate intensity duration frequency data for 27 different scenarios presented in Table 4

to create different realizations of future climate using different AOGCM responses. Appendix D presents the IDF data obtained using climate scenarios in terms of intensity.

The difference in the AOGCM scenarios relative to the historic perturbed scenario is summarized in Table 7.

Table 7: Percent Differences between Historic Perturbed, Wet and Dry Scenarios

ECHAM5AOM_A1B (Wet Scenario) and Historic Perturbed

Duration, min	Return Period, years					
	2	**5**	**10**	**25**	**50**	**100**
60	62.68	69.56	72.42	75.00	76.44	77.60
120	60.64	65.84	67.98	69.91	70.99	71.86
360	65.13	77.09	82.29	87.12	89.88	92.13
720	66.03	77.77	83.09	88.17	91.13	93.57
1440	63.22	72.99	77.42	81.63	84.07	86.09

MIROC3MEDRES_A2 (Dry Scenario) and Historic Perturbed

Duration, min	Return Periods, years					
	2	**5**	**10**	**25**	**50**	**100**
60	-6.79	-2.90	-1.28	0.18	0.99	1.65
120	-12.70	-15.09	-16.07	-16.96	-17.45	-17.85
360	-7.06	-6.60	-6.40	-6.21	-6.10	-6.02
720	-0.68	1.66	2.72	3.73	4.32	4.81
1440	-0.44	-0.10	0.05	0.20	0.28	0.35

The model results show variable results, with wide range of increase in extreme rainfall. ECHAM5AOM A1B appears to be the wettest while MIROC3.2MEDRES A2 being the driest of all. The wettest ECHAM5AOM A1B model shows more than 60% increase in rainfall compared to historic perturbed scenario. While the driest MIROC3.2 MEDRES A2 scenario shows slight decrease in precipitation intensity than the historic perturbed scenario. The difference between the wettest and the driest scenario ranges from 70% to 92% indicating huge range of uncertainty

among the realizations of AOGCMs. A comparison of different AOGCMs for specific duration
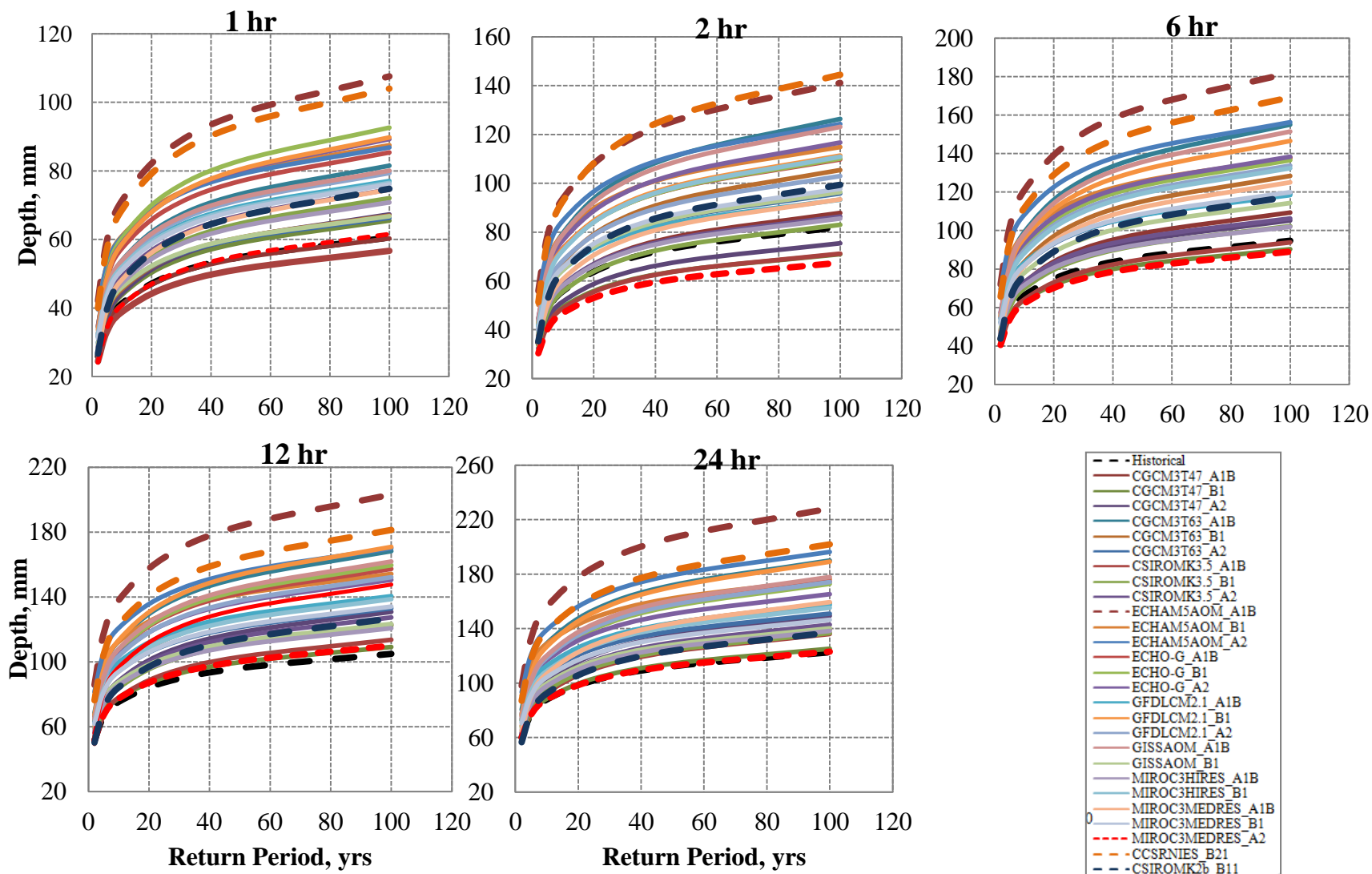
is presented in Figure 6.

Figure 6: IDF Plots of AOGCM Scenarios for Different Durations

4.5 Uncertainty Quantification of IDF Results

Because of the inherent uncertainties, the newly developed IDF curves from different AOGCMs are unable to provide an accurate estimate of future extreme rainfall, but they establish a significant fact: the future climate will not be the same as the historic one. Previous studies (Simonovic and Peck, 2009; Prodanovic and Simonovic, 2007) have generated updated IDF information for the City of London for 2050s (2041-2070) based on a single scenario (CCSRNIES B21) selected from the upper range of all scenarios presented in this study. In presence of uncertainties presented in section 4.4, adoption of one single scenario may suffer from under/over-estimation of the risks, which may have significant implications for the storm water management and design practice.

So, a kernel estimator based on the data driven plug-in approach described in section 3.2.6 is applied next to quantify the uncertainty arising from different AOGCM scenarios. Due to the fact that unlike other uncertainty estimation methods, kernel estimator provides variable weights at each point of interest, weights are calculated from the mean of all AOGCM data for presentation purpose. The weight function is calculated by modifying equation 3.18 as follows:

$$w(x, x_j, \lambda) = \frac{\dfrac{x - x_j}{\lambda}}{\sum_{j=1}^{n} \dfrac{x - x_j}{\lambda}}$$

where, for any time period t, x represents any data point within the ranges of generated data for which kernel estimator is applied, x_j is the AOGCM simulated data, λ is the plug-in bandwidth, and $j = 1, 2, \dots, n$ = number of AOGCM models and scenarios considered =27.

The mean of total sample size x_{ij} is considered as the data point from which the distance will be measured, where $i = 1, 2, ... t$ years of simulated IDF data= 117.

Figure 7 and Appendix E present the IDF curves incorporating the most useful information from the AOGCM scenarios. In this case, four scenarios have been selected: the 'historical perturbed' scenario as future state ignoring climate change, 'ECHAM5AOM A1B' scenario as the wettest scenario, 'MIROC3MEDRES A2' as the driest and the 'resultant' scenario as the scenario incorporating uncertainties from all AOGCM models and scenarios. The IDF curves of these selected scenarios for all durations for specific durations are presented in Appendix E. Table 9 presents the percent difference between the historical perturbed and resultant scenarios for 2080s. From the Table 9 it is seen that due to the changing climate, the intensity of rainfall is expected to increase by 20-40 % in 2071-2099.
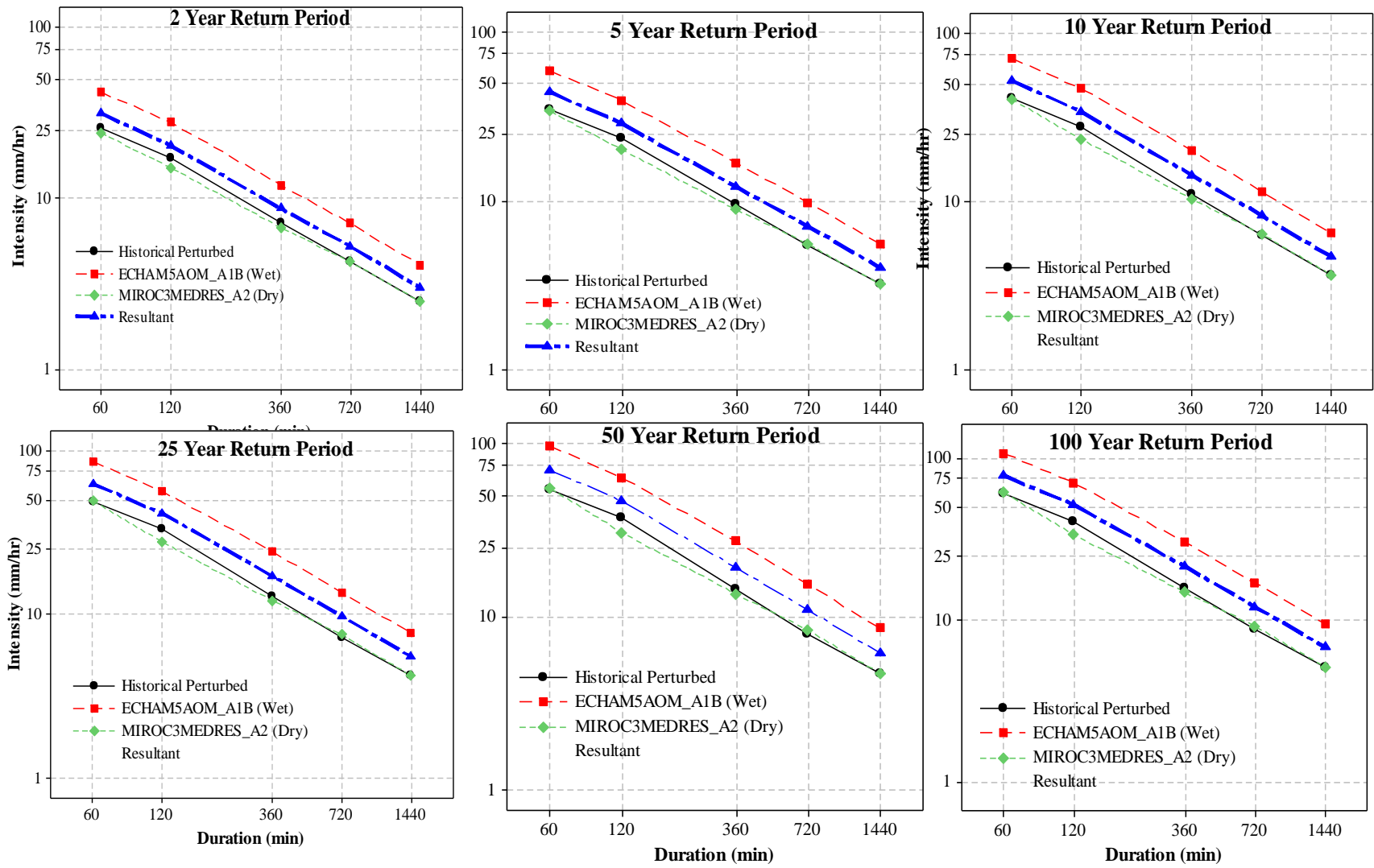
Figure 7: Comparison of IDF Plots for Different Scenarios

Table 9: Difference between Historical Perturbed and the 'Resultant' Scenario for 2080s

Duration (min)	Return Period, yrs					
	2	5	10	25	50	100
60	21.76	25.29	26.76	28.08	28.82	29.42
120	17.40	21.41	23.06	24.55	25.38	26.04
360	20.85	27.32	30.14	32.75	34.25	35.47
720	22.20	28.94	31.99	34.91	36.61	38.01
1440	20.63	25.77	28.10	30.32	31.60	32.67

Finally, the probabilities of extreme rainfall for all return periods are presented in terms of cumulative distribution plots. First, IDF plot of the resultant scenario is created (Figure 8).
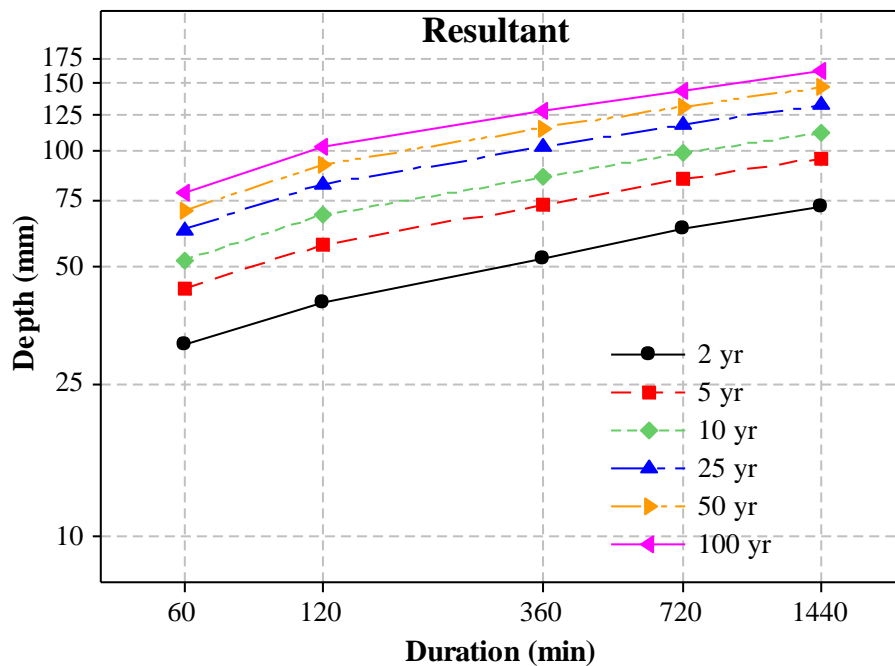
Figure 8: IDF Plot for Resultant Scenario

The cumulative distribution plots using the IDF from the AOGCM scenarios are plotted for all return periods and are presented in Figures 9 (a) and (b). Information from Figures

8 and 9 are combined to gather probabilities for any specific storm for any specific return period. For example, if the depth of 6 hour (360 min) storm for 5 year return period is 75 mm (Figure 8), the maximum probability of this specific storm can be counted as approximately 0.66 (Figure 9 and so on. This additional probability information will allow users to use the updated IDF information with more confidence.
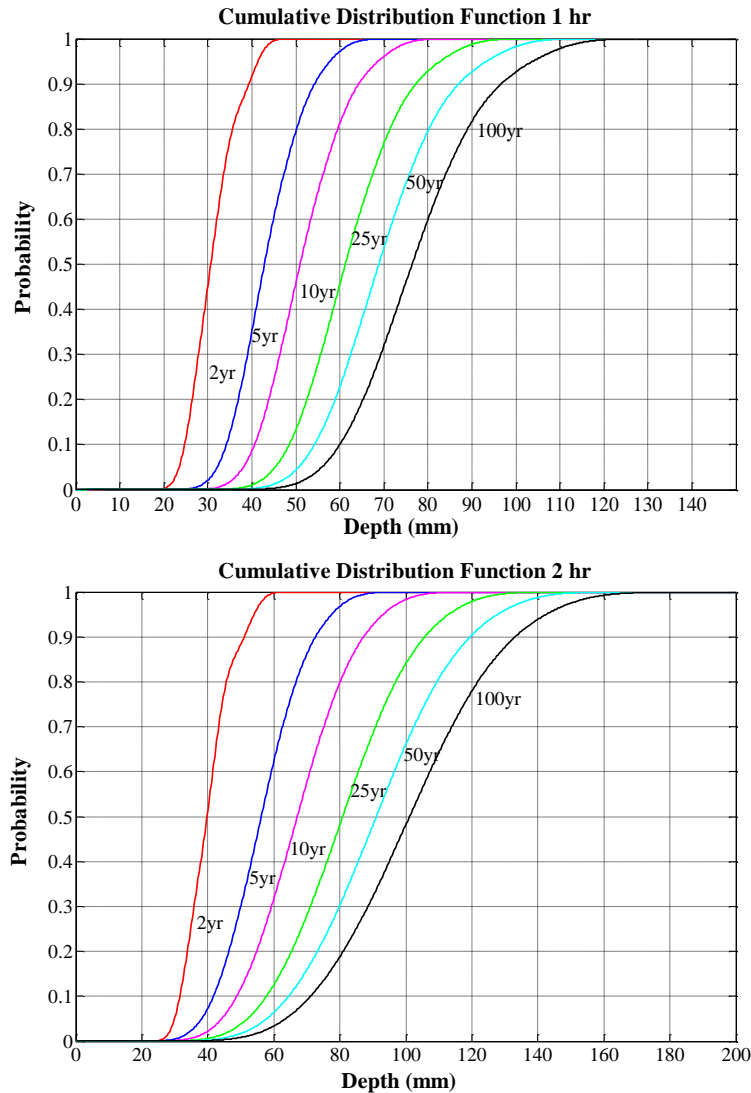
Figure 9 (a): Probability based IDF Curve of 1 and 2 Hour Duration
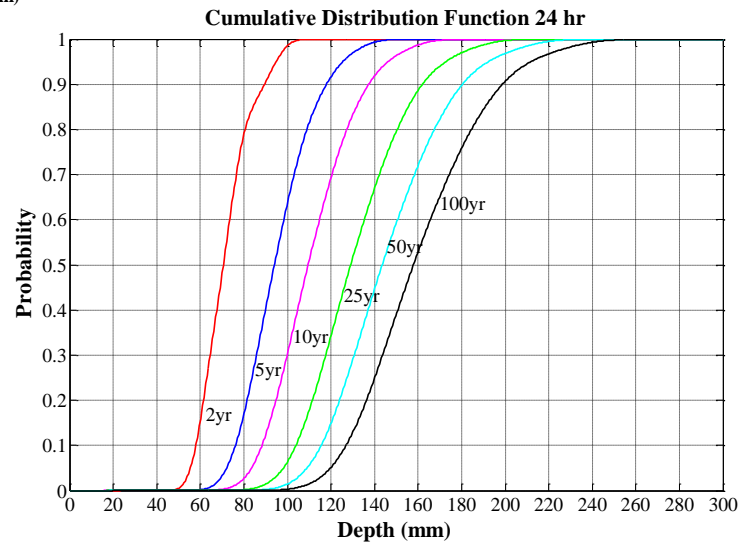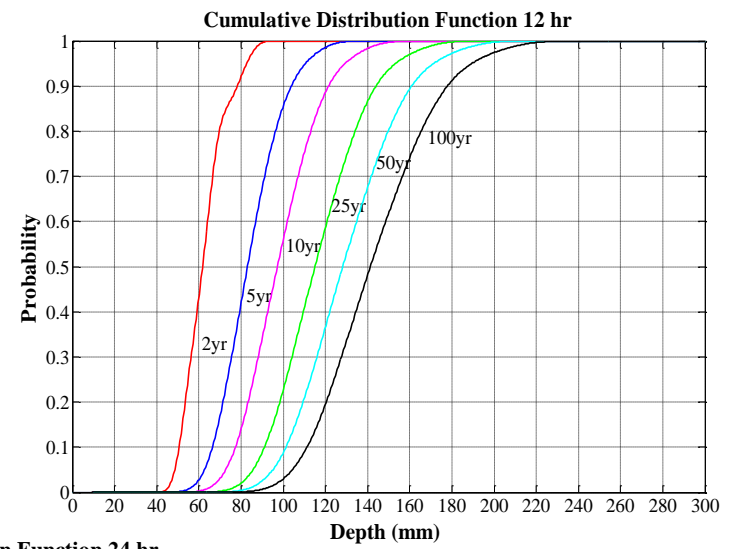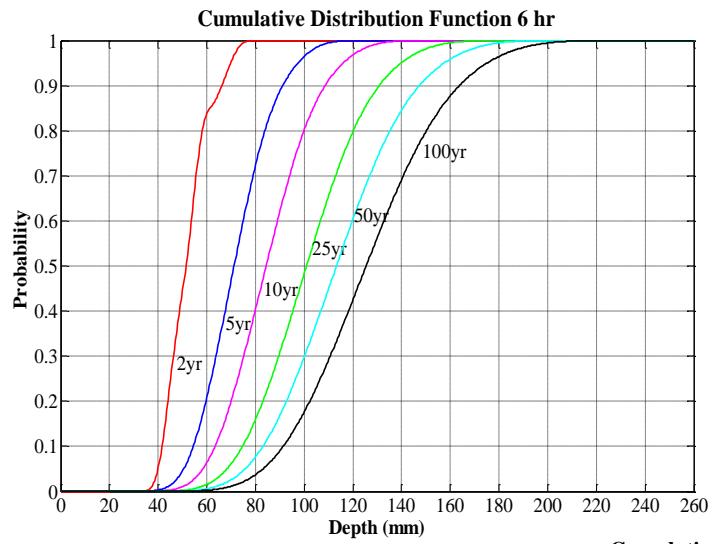
Figure 9 (b): Probability based IDF Curve of 6, 12, 24 Hour Duration

5. Conclusions

This study presents the methodology for updating of rainfall IDF curves for the City of London incorporating uncertainties associated with the use of different AOGCMs. The analysis of the annual maximum rainfall for developing intensity-duration-frequency plots for the City of London under climate change has resulted in important findings. Overall, two objectives have been achieved by this study: first, an extensive investigation of the possible realizations of future climate from 29 scenarios developed from AOGCM models and scenarios are performed using a downscaling based disaggregation approach. A nonparametric K-Nearest Neighbor multi-site weather generator operating on a daily time step is used to produce long sequence of rainfall data. The use of perturbation scheme has overcome the limitation of assumptions of stationarity by generating data beyond the range of the input. The downscaled daily outputs are disaggregated into hourly values by a non-parametric nearest neighbor based disaggregation scheme. Annual maximum series of rainfall are fitted to Gumbel distribution to develop IDF curves for 1, 2, 6, 12 and 24 hour durations for 2, 5, 10, 25, 50 and 100 years of return periods. Next, the associated uncertainties are estimated using non-parametric kernel estimation approach and the resultant IDF curve is developed based on a probabilistic approach.

The basic findings from the study are presented as follows:

- The rainfall patterns in the City of London will most certainly change in future due to climate change.

- Generation of future IDF information based on single site is limited. Incorporating a multi-site weather generator to produce sequences of future rainfall offers a more reliable approach for providing better spatial and temporal characteristics of rainfall patterns.

- Adoption of a single scenario for developing IDF information only provides a single realization of the future; application of a multi-model approach can provide more realistic information about the future climate.

- Use of the wettest or the driest scenario may be useful to capture the upper and lower bound scenario of the future climate change; however, single use of any of these scenarios may suffer from over/underestimation of the rainfall extremes with serious implications on storm water management practice and the development of design standards.

- Although the scenarios developed from different scenarios indicate large uncertainty associated with the global climate models, all of them indicate increase in intensity of future rainfall with a varying degree.

- A kernel based plug-in estimation approach is able to incorporate the uncertainties arising from different AOGCM models and to provide a more acceptable change in future rainfall extremes. The resultant scenario indicates approximately 20-40% changes in different duration rainfall for all return period.

- Use of a probability based intensity-duration-frequency curve is encouraged in order to apply the updated IDF information with higher level of confidence.

Acknowledgments

References

Adamowski, K. (1985). Nonparametric kernel estimation of flood frequencies, *Water Resources Research, 21 (11),* 1585-1590.

Allan, M. R., and W. J. Ingram (2002). Constraints on future changes in climate and the hydrologic cycle, *Nature, 419,* 224– 232.

Brissette, F., R. Leconte, M. Khalili (2007). Efficient stochastic generation of multi-site synthetic precipitation data. *Journal of Hydrology*, *345*,121-133.

Buishand, T. A. and Demare, G. R. (1990). Estimation of the Annual Maximum Distribution from Samples of Maxima n Separate Seasons. *Stochastic Hydrol. Hydraul. 4,* 89-103.

Buytaert, W., R. Ce´lleri, and L. Timbe (2009). Predicting climate change impacts on water resources in the tropical Andes: Effects of GCM uncertainty, *Geophysical Research Letters,36*, L07406, doi:10.1029/2008GL037048.

Coles S. (2001). *An Introduction to Statistical Modeling of Extreme Values*. London: Springer; 2001.

Coulibaly, P. and X. Shi. (2005). Identification of the Effect of Climate Change on Future Design Standards of Drainage Infrastructure in Ontario. Report prepared by McMaster University with funding from the Ministry of Transportation of Ontario. 82 pp.

Cubasch, U., G. A. Meehl, G. J. Boer, R. J. Stouffer, M. Dix, A. Noda, C. A. Senior, S. Raper, and K. S. Yap (2001). The Scientific Basic. Contribution of working group 1 to the Third Assessment Report of the Intergovernmental Panel of Climate Change, Cambridge University Press, Cambridge, UK and New York, USA, 881 pp.

CSA (2010). Development, Interpretation and Use of Rainfall Intensity- Duration-requency (IDF) Information: A Guideline for Canadian Water Resources Practitioners. 1st Edn., Canadian Standards Association, CSA PLUS 4013-10.

DAI Catalogue, (2009). Catalogue available datasets through DAI (Data Access and Integration), version 1.0, April 2009, Montreal, QC, Canada, 24 pp.

De Michele, C., Salvadori, G., (2005). Some hydrological applications of small sample estimators of generalized Pareto and extreme value distributions. *Journal of Hydrology 301,* 37–53.

Desramault, N. (2008). Estimation of Intensity Duration Frequency Curves for Current and Future Climates. Thesis submitted to the Graduate and Postdoctoral Studies Office in partial fulfilments of requirements of the degree of Master of Engineering Department, McGill University, Montreal, Québec, Canada. 75 pp.

Efromovich, S. (1999). *Nonparametric Curve Estimation: Methods, Theory, and Applications*, Springer, New York.

Eum, H. I., Arunachalam, V. and Simonovic, S. P. (2009). Integrated Reservoir Management System for Adaptation to Climate Change Impacts in the Upper Thames River Basin. Water Resources Research Report no. 062, Facility for Intelligent Decision Support, Department of Civil and Environmental Engineering, London, Ontario, Canada, 81 pages. ISBN: (print) 978-0-7714-2710-7; (online) 978-0-7714-2711-4.

Hall, P., and Marron, J. S. (1991). Lower Bounds for Bandwidth Selection in Density Estimation, *Probability Theory and Related Fields, 90,* 149-173.

Huard, D., Mailhot, A., and Duchesne, S. (2010). Bayesian Estimation of Intensity-Duration-Frequency Curves and of the Return Period Associated to a Given Rainfall Event. *Stoch. Environ. Res. Risk. Assess., 2,* 337-347.

Hughes, J. P., and P. Guttorp (1994). A class of stochastic models for relating synoptic atmospheric patterns to regional hydrologic phenomena, *Water Resources Research, 30(5),* 1535–1546.

IPCC (2007). Climate Change 2007: The Physical Science Basis. Contribution of working group 1 to the Fourth Assessment Report of the Intergovernmental Panel of Climate Change, Annexes [Baede, A.P.M. (ed.)]. Cambridge University Press, Cambridge UK and New York, USA, 48pp.

Jaruskova, D. and Hanek, M. (2006). Peak Over Threshold method in Comparison with Block Maxima Method for Estimating High Return Levels of Several Northern Moravia Precipitation and Discharges Series. *J. Hydrol. Hydromech., 4,* 309-319.

Jarvis, C.S. et al., (1936). Floods in the United States, Magnitudes and Frequency. USGS Water Supply Paper 771, Washington, DC.

Jones, M.C., J. S. Marron, and S. J. Sheather (1996). A brief survey of bandwidth selection for density estimation, *Journal of the American Statistical Association, 91(433),* 401–407.

Katz, R. W., Parlange, M. B. and Naveau, P. (2002). Statistics of Extremes in Hydrology. *Advances in Water Resources, 25,* 1287-1304.

Lall, U. (1995). Nonparametric Function Estimation: Recent Hydrologic Contributions. Reviews of Geophysics, Contributions in Hydrology, U.S. National Report to the IUGG 1991-1994, 1093-1099.

Lall, U., B. Rajagopalan and D. G. Tarboton (1996). A Nonparametric Wet/Dry Spell Model

for Daily Precipitation, *Water Resources Research, 32(9),* 2803-2823.

Langbein, W.B., (1949). Annual floods and the partial duration flood series. *Transactions of AGU 30,* 879–881.

Madsen, H., Rosbjerg, D., (1997). Generalized least squares and empirical Bayes estimation in regional partial duration series index-flood modeling. *Water Resources Research 33 (4),* 771–781.

Mailhot, A. and Duchesne, S. (2010). Design criteria of urban drainage infrastructures under climate change, *J Water Resour Plann Manage 136,* 201–208.

Mailhot, A., Duchesne,S., .Rivard, G., Nantel, E., Caya, D., and Villeneuve, J.-P. (2006). Climate change impacts on the performance of urban drainage systems for Southern Québec. *Proceedings of EIC Climate Change Technology Conference*, Ottawa, Ontario, Canada.

Mansour, R. and Burn, D. H. (2010). Weather Generator and Hourly Disaggregation Model. Department of Civil Engineering, University of Waterloo, Waterloo, Ontario, Canada.

Mailhot, A., Duchesne,S., Caya, D., and Talbot, G. (2007). Assessment of future change in intensity–duration–frequency (IDF) curves for Southern Quebec using the Canadian Regional Climate Model (CRCM). *Journal of Hydrology*, *347 (1-2),* 197-210.

Mehdi, B., Mrena, C., and Douglas, A. (2006). Adapting to climate change: An introduction for Canadian Municipalities. Canadian Climate Impacts and Adaptation Research Network (C-CIARN), http://www.c-ciarn.ca/.

MTO (1997). Ministry of Transportation of Ontario Drainage Management Manual. Drainage and Hydrology Section, Transportation Engineering Branch, and Quality Standards Division, Ministry of Transportation of Ontario, Ottawa, Ontario, Canada.

Nakicenovic, N., Alcamo, J., Davis, G., de Vries, B., Fenhann, J., and co-authors. (2000). IPCC Special Report on Emissions Scenarios. *UNEP/GRID-Ardenal Publications*.

New, M., and M. Hulme, (2000), Representing uncertainty in climate change scenarios: a Monte-Carlo approach, *Integrated Assessment, 1,* 203-213.

Nguyen, T-D., V-T-V. Nguyen, and P. Gachon. (2007*a*). A spatial-temporal downscaling approach for construction of intensity-duration-frequency curves in consideration of GCM-based climate change scenarios. *Advances in Geosciences*, *6,* 11-21.

Nguyen, V-T-V., T-D. Nguyen and A. Cung. (2007*b*). A statistical approach to downscaling of sub-daily extreme rainfall processes for climate-related impacts studies in urban areas. *Water Science and Technology: Water Supply*, **7** (2), 183-192.

Onof, C., Arnbjerg-Nielsen, K., (2009). Quantification of anticipated future changes in high resolution design rainfall for urban areas. Atmospheric Research 92, 350–363. doi:10.1016/j.atmosres.2009.01.014.

Park, B. U. and Marron, J. S. (1990) Comparison of data-driven bandwidth selectors. J. Am. Statist. Ass., 85, 66-72.

Predrag Prodanovic and Slobodan P. Simonovic (2007). Development of rainfall intensity duration frequency curves for the City of London under the changing climate. Water Resources Research Report no. 058, Facility for Intelligent Decision Support, Department of Civil and Environmental Engineering, London, Ontario, Canada, 51 pages. ISBN: (print) 978-0-7714-2667-4; (online) 978-0-7714-2668-1.

Prudhomme, C., D. Jakob, and C. Svensson (2003). Uncertainty and climate change impact on the flood regime of small UK catchments, *Journal of Hydrology, 277,* 1 – 23.

Rasmussen, P.F., Ashkar, F., Rosbjerg, D., Bobee, B., (1994). The POT method for flood estimation: a review. In: Hipel, K.W. (Ed.), Stochastic and Statistical Methods in Hydrology and Environmental Engineering, Extreme Values: Floods and Droughts, vol. 1. Kluwer, Dordrecht, NL, pp. 15–26.

Rosenblatt (1956). Remarks on some nonparametric estimates of a density function. *Ann. Math. Statist. 27,* 832-837.

Scott, D. W., and G. R. Terrell, (1987). Biased and Unbiased Cross- Validation in Density Estimation, *Journal of the American Statistical Association, 82,* 1131-1146.

Sharif, M., Burn, D. H. and Wey, K.M. (2007). Daily and Hourly weather generation using a K-Nearest Neighbor Approach, 18th CSCE Hydrotechnical Conference, August 2007, Winnipeg, MB, 1 - 10.

Sharif, M., and D. H. Burn (2006). Simulating climate change scenarios using an improved K-nearest neighbor model, *Journal of hydrology, 325,* 179-196.

Sharma, A., D. G. Tarbaton, and U. Lall, (1997). Streamflow simulation − a nonparametric approach, *Water Resources Research, 33 (2),* 291-308.

Sheather, S. J. (1983). A Data-Based Algorithm for Choosing the Window Width When Estimating the Density at a Point, *Computational Statistics and Data Analysis, 1,* 229-238.

Sheather, S. J. (1986). An Improved Data-Based Algorithm for Choosing the Window Width When Estimating the Density at a Point, *Computational Statistics and Data Analysis, 4, 61-65.*

Sheather, S. J., and M. C. Jones (1991). A Reliable Data-Based Bandwidth Selection Method for Kernel Density Estimation, *Journal of the Royal Statistical Society, Ser. B, 53,* 683-690.

Silverman, B. W. (1986). *Density estimation for statistics and data analysis. Monographs on Statistics and Applied Probability*, Chapman & Hall/ CRC., Washington, D.C.

Slobodan P. Simonovic and Angela Peck (2009). Updated rainfall intensity duration frequency curves for the City of London under the changing climate. Water Resources Research Report no. 065, Facility for Intelligent Decision Support, Department of Civil and Environmental Engineering, London, Ontario, Canada, 64 pages. ISBN: (print) 978-0-7714-2819-7; (online) 978-0-7714-2820-3.

Smith, R. L., Tebaldi, C., Nychka, D., and Mearns, L (2009). Bayesian modeling of uncertainty in ensembles of climate models, *Journal of the American Statistical Association, 104 (485),* 97-116., doi:10.1198/jasa.2009.0007.

Smith, R.L., (2003). Statistics of extremes, with applications in environment, insurance and finance. <http://www.stat.unc.edu/postscript/rs/semstatrls.ps>.

Solaiman and Simonovic (2011). Quantifying Uncertainties in the Modelled Estimates of Extreme Precipitation Events at Upper Thames River Basin. Water Resources Research Report no. 067, Facility for Intelligent Decision Support, Department of Civil and Environmental Engineering, London, Ontario, Canada, 64 pages.

Stainforth, D. A., T. E. Downing, R. W. A. Lopez, and M. New (2007). Issues in the interpretation of climate model ensembles to inform decisions, *Philos. Trans. R. Soc., Ser. A, 365,* 2163–2177.

Stone, D.A., Weaver, A.J., Zwiers, F.W., (2000). Trend in Canadian precipitation intensity. *Atmos. Ocean 38 (2),* 321–347.

Svensson, C., Clarke, R., Jones, D. (2007). An Experimental Comparison of Methods for Estimating Rainfall Intensity-Duration-Frequency Relations from Fragmantory Methods. *Journal of Hydrology, 341*, 79-89.

Taesombat, V., Yevjevich, V., 1978. Use of partial flood series for estimating distribution of maximum annual flood peak. Hydrology Papers #97, Colorado State University, Fort Collins, CO.

Trigo, R.M. and J.P. Palutikof (2001). Precipitation scenarios over Iberia: a comparison between direct GCM output and different downscaling techniques. *J. Climate 14*, 4422-4446.

Vincent, L.A., and E. Mekis (2006). Changes in daily and extreme temperature and precipitation indices for Canada over the twentieth century. *Atmosphere-Ocean, 44(2),* 177- 193.

Widmann M, Bretherton CS, Salathe-Jr EP. (2003). Statistical precipitation downscaling over the North-western United States using numerically simulated precipitation as a predictor. *Journal of Climate 16(5),* 799-816.

Wilby, R. L., and I. Harris (2006). A framework for assessing uncertainties in climate change impacts: Low-flow scenarios for the River Thames, UK, *Water Resources Research, 42,* W02419, doi: 10.1029/2005WR004065.

APPENDIX A: Regression Test Results

Regression Results for Stations Within 0-200 km Radius Distance

Predictor	t-Statistic	Probability (p)
Hamilton RBG	-8.52	0.000
Hamilton A	20.54	0.000
Fergus	-3.91	0.000
Elora	-4.17	0.000
Delhi	10.71	0.000
Chatham WPCP	**0.27**	**0.791**
Brantford MOE	-6.15	0.000
Woodstock	26.58	0.000
Waterloo A	28.64	0.000
St. Thomas WPCP	10.53	0.000
Stratford MOE	8.06	0.000
Sarnia	25.15	0.000
Barrie	3.92	0.000
Owensound	**-2.82**	**0.005**
Wiarton	7.49	0.000
Toronto City	-4.75	0.000
Toronto Int'l A	4.69	0.000

Regression Results for Stations Within 0-175 km Radius Distance

Predictor	t-Statistic	Probability (p)
Woodstock	26.43	0.000
St. Thomas WPCP	9.97	0.000
Stratford MOE	8.34	0.000
Delhi	10.81	0.000
Brantford MOE	-6.42	0.000
Waterloo A	29.85	0.000
Sarnia	25.80	0.000
Elora	-4.05	0.000
Hamilton A	21.40	0.000
Hamilton RBG	-11.24	0.000
Fergus	-3.96	0.000
Chatham WPCP	**0.22**	**0.829**
Toronto Int'l A	4.29	0.000
Owensound	**2.38**	**0.017**

Regression Results for Stations Within 0-150 km Radius Distance

Predictor	t-Statistic	Probability (p)
Woodstock	26.36	0.000
St. Thomas WPCP	9.96	0.000
Stratford MOE	8.92	0.000
Delhi	10.83	0.000
Brantford MOE	-6.50	0.000
Waterloo A	29.82	0.000
Sarnia	25.97	0.000
Elora	-4.01	0.000
Hamilton A	21.43	0.000
Hamilton RBG	-11.26	0.000
Fergus	-3.62	0.000
Chatham WPCP	**0.33**	**0.743**
Toronto Int'l A	4.36	0.000

Regression Results for Stations Within 0-125 km Radius Distance

Predictor	t-Statistic	Probability (p)
Woodstock	26.30	0.000
St. Thomas WPCP	9.86	0.000
Stratford MOE	8.77	0.000
Delhi	10.63	0.000
Brantford MOE	-6.76	0.000
Waterloo A	34.25	0.000
Sarnia	26.30	0.000
Elora	-3.68	0.000
Hamilton A	23.70	0.000
Hamilton RBG	-10.81	0.000
Fergus	**-3.30**	**0.001**
Chatham WPCP	**0.19**	**0.853**

Regression Results for Stations Within 0-100 km Radius Distance

Predictor	t-Statistic	Probability (p)
Woodstock	25.76	0.000
St. Thomas WPCP	10.17	0.000
Stratford MOE	7.79	0.000
Delhi	9.41	0.000
Brantford MOE	-10.98	0.000
Waterloo A	34.39	0.000
Sarnia	25.85	0.000
Elora	-8.26	0.000
Hamilton A	21.60	0.000

Regression Results for Stations Within 0-75 km Radius Distance

Predictor	t-Statistic	Probability (p)
Woodstock	30.19	0.000
St. Thomas WPCP	10.22	0.000
Stratford MOE	13.99	0.000
Delhi	15.71	0.000
Brantford MOE	2.27	0.023

Regression Results for Stations Within 0-50 km Radius Distance

Predictor	t-Statistic	Probability (p)
Woodstock	40.28	0.000
St. Thomas WPCP	19.86	0.000
Stratford MOE	16.68	0.000

APPENDIX B: SRES Emission Scenarios
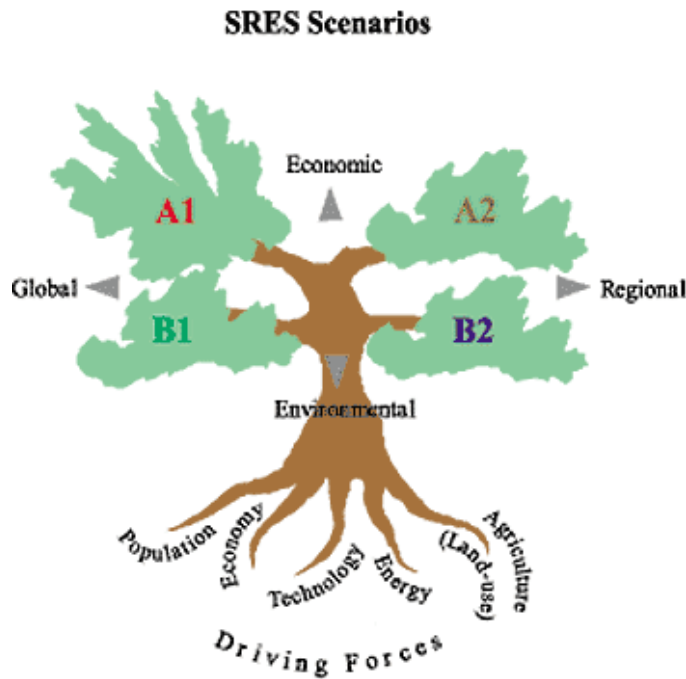
Figure A1: SRES Emission Scenarios (Nakicenovic et al, 2000)

A1B: In scenario A1B, the storyline includes rapid economic expansion and globalization, a population peaking at 9 billion in 2050, and a balanced emphasis on a wide range of energy sources (Nakicenovic et al, 2000).

B1: The storyline for the B1 scenario is much like A1B in terms of population and globalization; however there are changes toward a service and information economy with more resource efficient and clean technologies. Emphasis is put on finding global solutions for sustainability (Nakicenovic et al, 2000).

A2: For scenario A2, the storyline consists of a world of independently operating nations with a constantly increasing population and economic development on a regional level.

Technological advances in this storyline occur more slowly due to the divisions between

nations (Nakicenovic et al, 2000).

APPENDIX C: Atmosphere-Ocean General Circulation Models

Criteria for Selecting Climate Scenarios

Five criteria that should be met by climate scenarios if they are to be useful for impact researchers and policy makers are suggested by IPCC and are quoted here:

- *Criterion 1: Consistency with global projections. They should be consistent with a broad range of global warming projections based on increased concentrations of greenhouse gases. This range is variously cited as 1.4°C to 5.8°C by 2100, or 1.5°C to 4.5°C for a doubling of atmospheric CO2 concentration (otherwise known as the "equilibrium climate sensitivity").*

- *Criterion 2: Physical plausibility. They should be physically plausible; that is, they should not violate the basic laws of physics. Hence, changes in one region should be physically consistent with those in another region and globally. In addition, the combination of changes in different variables (which are often correlated with each other) should be physically consistent.*

- *Criterion 3: Applicability in impact assessments. They should describe changes in a sufficient number of variables on a spatial and temporal scale that allows for impact assessment. For example, impact models may require input data on variables such as precipitation, solar radiation, temperature, humidity and wind speed at spatial scales ranging from global to site and at temporal scales ranging from annual means to daily or hourly values.*

- *Criterion 4: Representative. They should be representative of the potential range of future regional climate change. Only in this way can a realistic range of possible impacts be estimated.*

- *Criterion 5: Accessibility. They should be straightforward to obtain, interpret and apply for impact assessment. Many impact assessment projects include a separate scenario*

development component which specifically aims to address this last point. The DDC and this guidance document are also designed to help meet this need.

Challenges in using AOGCMs

GCMs depict the climate using a three dimensional grid over the globe (Figure), typically having a horizontal resolution of between 250 and 600 km, 10 to 20 vertical layers in the atmosphere and sometimes as many as 30 layers in the oceans. Their resolution is thus quite coarse relative to the scale of exposure units in most impact assessments, hence only partially fulfilling criterion 3. Moreover, many physical processes, such as those related to clouds, also occur at smaller scales and cannot be properly modeled. Instead, their known properties must be averaged over the larger scale in a technique known as parameterization. This is one source of uncertainty in GCM-based simulations of future climate. Others relate to the simulation of various feedback mechanisms in models concerning, for example, water vapor and warming, clouds and radiation, ocean circulation and ice and snow albedo. For this reason, GCMs may simulate quite different responses to the same forcing, simply because of the way certain processes and feedbacks are modeled.

However, while these differences in response are usually consistent with the climate sensitivity range described in criterion 1, they are unlikely to satisfy criterion 4 concerning the uncertainty range of regional projections. Even the selection of all the available GCM experiments would not guarantee a representative range, due to other uncertainties that GCMs do not fully address, especially the range in estimates of future atmospheric composition.
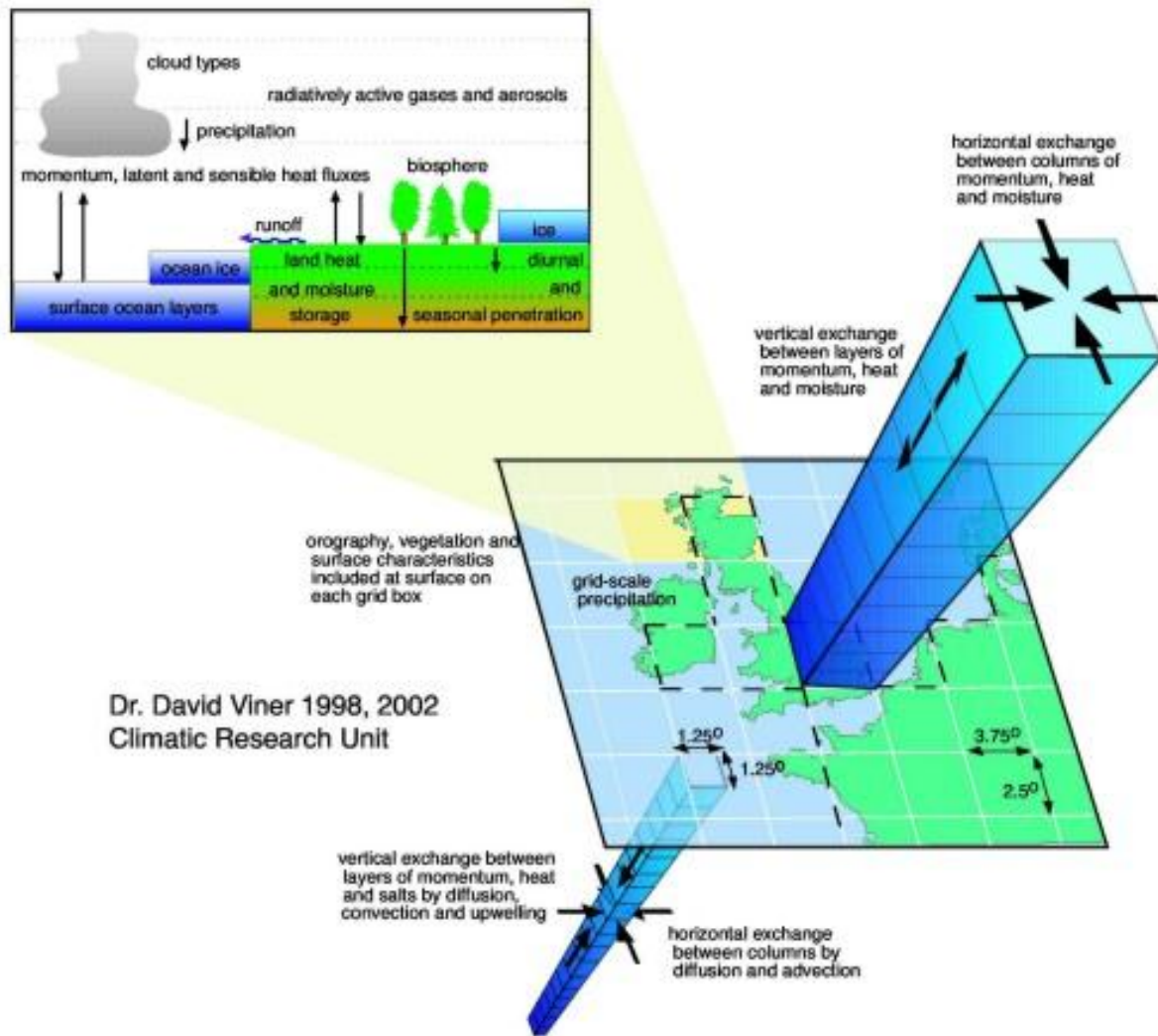
Figure: 3-Dimensional Representation of Climate Models (Climate Research Unit website, 2011)

(from http://www.cru.uea.ac.uk/cru/info/modelcc/ retrieved on 3/01/2011)

Canadian Coupled Global Climate Model

The third generation Coupled Global Climate Model (CGCM3) was created in 2005 by the Canadian Centre for Climate Modelling and Analysis (CCCma) in Victoria, BC for use in the IPCC 4th assessment report to run complex mathematical equations which describe the earth's atmospheric and oceanic processes. The CGCM3 climate model includes four major components: an atmospheric general circulation model, an ocean general circulation model, a thermodynamic sea-ice model, and a land surface model (Hengeveld, 2000) and consists of two resolutions, T47 and T63. The T47 version has a surface grid whose spatial resolution is roughly 3.75 degrees lat/lon and 31 levels in the vertical. The ocean grid shares the same land mask as the atmosphere, but has four ocean grid cells underlying every atmospheric grid cell. The ocean resolution in this case is roughly 1.85 degrees, with 29 levels in the vertical.

The T63 version has a surface grid whose spatial resolution is roughly 2.8 degrees latitude/longitude and 31 levels in the vertical. As before the ocean grid shares the same land mask as the atmosphere, but in this case there are 6 ocean grids underlying every atmospheric grid cell. The ocean resolution is therefore approximately 1.4 degrees in longitude and 0.94 degrees in latitude. This provides slightly better resolution of zonal currents in the Tropics, more nearly isotropic resolution at mid latitudes, and somewhat reduced problems with converging meridians in the Arctic.

(Compiled from http://www.ec.gc.ca/ccmac-cccma/default.asp?lang=En&n=1299529F-1)

Commonwealth Scientific and Industrial Research Organization's Mk3.5 Climate Systems Model

Australia's Commonwealth Scientific and Industrial Research Organization created the AOGCM CSIROMK3.5, which is an improved version of the MK climate systems model. The model consists of several components: atmosphere, land surface, ocean and polar ice. The dynamic framework of the atmospheric model is based upon the spectral method with the equations cast in the flux form that conservs predicted variables. The atmospheric moisture variables (vapour, water and ice) are advected by a Semi-Lagrangian Transport (SLT) algorithm (McGregor 1993). The most recent version (MK3.5) has included a representation of the Great Lakes and changes in land surface scheme and it's representation of surface albedo under freezing than it's previous versions. The MK3.5 version provides improved information by including the spatially varying eddy transfer coefficients (Visbeck et al, 1997) and the Kraus-Turner mixed layer (1967) scheme. Improvements have also been done in it's oceanic behavior in the high latitude Southern ocean, where the stratification and circulation are generally more realistic than the prior models. The spatial resolution of the model is 1.875×1.875.

Compiled from (http://www.cawcr.gov.au/publications/technicalreports/CTR_021.pdf)

Max Planck Institute for Meteorology's ECHAM5AOM Model

ECHAM5 is the 5th generation of the ECHAM general circulation model. Depending on the configuration the model resolves the atmosphere up to 10 hPa for tropospheric studies, or up to 0.01 hPa for middle atmosphere studies. The current version differ in the vertical extent of the atmosphere as well as the relevant processes than it's earlier versions. It is capable of hosting sub-models (chemistry, aerosol and vegetation) going beyond the meteorological processes of a AOGCM. The model can be used as a part of a coupled ocean GCM, in assimilation by linear relaxation and as a standalone column model.

For integrations to start, the model requires several files. These file contain information for the description of the initial or re-start state of the atmosphere (boundary conditions at the surface, the ozone distribution and tables of constants of LW radiation schemes), the description of assumed conditions during the integration, e.g. sea surface temperature, or the initialization of parameterizations.

(Compiled from http://www.mpimet.mpg.de/en/science/models/echam/echam5.html)

Meteorological Institute, University of Bonn Meteorological Research Institute of KMA Model and Data Groupe at MPI-M's ECHO-G Model

The climate model ECHO-G (Legutke and Voss, 1999) is a coupled climate model consisting of the atmospheric model ECHAM4 (Roeckner et al., 1996) and the ocean model HOPE (Wolff et al., 1997).

The ECHAM4-model is based on primitive equations. The prognostic variables are vorticity, divergence, logarithm of surface pressure, temperature, specific humidity, mixing ratio of total cloud water and optionally a number of trace gases and aerosols.The vertical extension is up to a pressure level of 10 hPa, which corresponds to a height of approximately 30km. A hybrid sigma-pressure coordinate system is used with 19 irregularly ordered levels and with highest resolution in the atmospheric boundary layer. The bottom level is placed at a height of about 30m above the surface corresponding approximately to the surface layer. In this study the ECHAM4 model has a horizontal resolution of about 3.75lat x 3.75lon.

The ocean model HOPE (Hamburg Ocean Primitive Equation) is an ocean general circulation model (OGCM) based on primitive equations with the representation of thermodynamic processes. It is a non-eddy resolving circulation model. HOPE-G has a horizontal resolution of approximately 2.8lat x 2.8lon with a grid refinement in the tropical regions over a band from 10N to 10S. This meridional grid refinement reaches a value of 0.5 at the equator allowing for a more realistic representation of ENSO variability in the tropical Pacific Ocean . The ocean model has 20 vertical, irregularly ordered layers.

The coupling as well as the interpolation between the atmosphere and the ocean model is controlled by the coupling software OASIS (Terray et al., 1998). Concerning the coupling

dynamics, at a distinct frequency the atmospheric component of the model passes heat, fresh water and momentum to the ocean and gets information about surface conditions of the ocean. This frequency is equal for all exchange fields and describes a 'coupled time step'. The fields that are exchanged are averaged over the last coupled time step. Further aspects of the exchange processes are flux corrections due to the interactive coupling between ocean and atmosphere in order to prevent climate drift. These heat- and freshwater fluxes were diagnosed in a coupled spin-up integration. Accordingly, the sea-surface-temperature and sea-surface salinity were restored to their climatological observed values. This flux adjustment is constant in time and its global average vanishes.

Quoted from (http://coast.gkss.de/staff/wagner/midhol/model/model_des.html)

Goddard Institute for Space Studies' Atmospheric Ocean Model

The North American Space Association and the Goddard Institute for Space Studies developed the GISS-AOM climate model, first in 1995 and then a revised version was created with smaller grids in 2004 for the IPCC 4th assessment report. The model requires two kinds of input, specified parameters and prognostic variables, and generates two kinds of output, climate diagnostics and prognostic variables. The specified input parameters include physical constants, the Earth's orbital parameters, the Earth's atmospheric constituents, the Earth's topography, the Earth's surface distribution of ocean, glacial ice, or vegetation, and many others. The time varying prognostic variables include fluid mass, horizontal velocity, heat, water vapor, salt, and subsurface mass and energy fields. The resolution for the model is 4° longitude by 3° latitude (PCMDI, 2005). The atmospheric grid has 12 vertical layers (PCMDI, 2005).

Model for Interdisciplinary Research on Climate version 3.2

The Japanese Model for Interdisciplinary Research on Climate version 3.2 (MIROC3.2) was developed in two resolutions: the high resolution (MIROC3.2HIRES) in 1.125° × 1.125° grid and the medium resolution (MIROC3.2MEDRES) in 2.8° × 2.8° grid. For present study, two emissions scenarios from MIROC3.2HIRES (A1B and B1) and three scenarios (A1B, A2 and B1) from MIROC3.2MEDRES were used.

APPENDIX D: Comparison of Future IDF Results in terms of Intensities (mm/hr)

Historic Perturbed	Return Periods, T yrs					
Duration (min)	2 yr	5 yr	10 yr	25 yr	50 yr	100 yr
60	25.87	35.16	41.32	49.09	54.85	60.57
120	17.39	23.73	27.92	33.22	37.16	41.06
360	7.26	9.54	11.05	12.96	14.38	15.78
720	4.31	5.49	6.28	7.28	8.01	8.75
1440	2.50	3.20	3.66	4.25	4.68	5.11

CGCM3T47_A1B	Return Periods, T yrs					
Duration (min)	2 yr	5 yr	10 yr	25 yr	50 yr	100 yr
60	25.53	34.84	41.00	48.79	54.57	60.31
120	16.95	24.17	28.96	35.00	39.48	43.94
360	7.28	10.21	12.15	14.60	16.42	18.23
720	4.43	5.98	7.02	8.32	9.29	10.25
1440	2.54	3.42	4.00	4.73	5.28	5.82

CGCM3T47_B1	Return Periods, T yrs					
Duration (min)	2 yr	5 yr	10 yr	25 yr	50 yr	100 yr
60	26.38	36.86	43.80	52.56	59.06	65.52
120	16.08	21.28	24.71	29.05	32.28	35.47
360	7.06	9.20	10.62	12.41	13.73	15.05
720	4.34	5.61	6.46	7.52	8.31	9.10
1440	2.46	3.20	3.69	4.31	4.76	5.22

CGCM3T47_A2	Return Periods, T yrs					
Duration (min)	2 yr	5 yr	10 yr	25 yr	50 yr	100 yr
60	25.77	36.90	44.26	53.57	60.47	67.32
120	16.25	22.00	25.80	30.61	34.17	37.71
360	7.21	9.98	11.81	14.12	15.84	17.54
720	4.51	6.22	7.35	8.79	9.85	10.91
1440	2.61	3.58	4.22	5.03	5.63	6.22

CGCM3T63_A1B	Return Periods, T yrs					
Duration (min)	2 yr	5 yr	10 yr	25 yr	50 yr	100 yr
60	31.57	44.95	53.80	64.99	73.30	81.53
120	21.14	32.40	39.85	49.27	56.25	63.19
360	9.07	13.56	16.53	20.29	23.08	25.84
720	5.70	7.93	9.41	11.27	12.65	14.02
1440	3.35	4.57	5.38	6.41	7.16	7.92

CGCM3T63_B1	Return Periods, T yrs					
Duration (min)	2 yr	5 yr	10 yr	25 yr	50 yr	100 yr
60	28.35	38.69	45.53	54.18	60.60	66.96
120	18.81	27.89	33.90	41.49	47.12	52.71
360	7.96	11.56	13.94	16.95	19.19	21.40
720	4.95	6.75	7.94	9.44	10.56	11.67
1440	2.85	3.86	4.53	5.37	6.00	6.62

CGCM3T63_A2	Return Periods, T yrs					
Duration (min)	2 yr	5 yr	10 yr	25 yr	50 yr	100 yr
60	29.92	39.66	46.11	54.26	60.31	66.31
120	19.95	27.44	32.40	38.66	43.31	47.92
360	8.69	11.68	13.66	16.16	18.02	19.86
720	5.27	6.82	7.86	9.16	10.13	11.09
1440	3.04	3.91	4.48	5.21	5.75	6.29

CSIROMK3.5_A1B	Return Periods, T yrs					
Duration (min)	2 yr	5 yr	10 yr	25 yr	50 yr	100 yr
60	24.45	33.08	38.80	46.02	51.38	56.70
120	15.40	20.81	24.38	28.91	32.26	35.59
360	6.72	9.11	10.69	12.69	14.17	15.64
720	4.12	5.55	6.50	7.70	8.59	9.47
1440	2.42	3.29	3.86	4.59	5.13	5.67

CSIROMK3.5_B1	Return Periods, T yrs					
Duration (min)	2 yr	5 yr	10 yr	25 yr	50 yr	100 yr
60	27.45	39.40	47.30	57.29	64.71	72.06
120	16.86	23.46	27.82	33.34	37.44	41.50
360	7.30	9.91	11.64	13.82	15.44	17.05
720	4.43	5.97	6.99	8.28	9.24	10.19
1440	2.53	3.38	3.94	4.65	5.17	5.70

CSIROMK3.5_A2	Return Periods, T yrs					
Duration (min)	2 yr	5 yr	10 yr	25 yr	50 yr	100 yr
60	28.73	41.01	49.13	59.40	67.02	74.59
120	18.13	24.83	29.28	34.89	39.05	43.18
360	7.76	10.42	12.19	14.42	16.07	17.72
720	4.70	6.29	7.34	8.66	9.64	10.62
1440	2.64	3.53	4.12	4.86	5.41	5.95

ECHAM5AOM_A1B	Return Periods, T yrs					
Duration (min)	2 yr	5 yr	10 yr	25 yr	50 yr	100 yr
60	42.09	59.63	71.23	85.90	96.78	107.58
120	27.94	39.35	46.91	56.45	63.53	70.56
360	11.99	16.90	20.15	24.26	27.30	30.33
720	7.15	9.77	11.50	13.69	15.32	16.93
1440	4.09	5.54	6.50	7.71	8.61	9.51

ECHAM5AOM_B1	Return Periods, T yrs					
Duration (min)	2 yr	5 yr	10 yr	25 yr	50 yr	100 yr
60	39.63	52.45	60.94	71.66	79.62	87.52
120	25.10	33.75	39.48	46.72	52.09	57.42
360	10.91	14.13	16.26	18.95	20.95	22.93
720	6.58	8.26	9.37	10.78	11.82	12.85
1440	3.78	4.74	5.37	6.17	6.76	7.35

ECHAM5AOM_A2	Return Periods, T yrs					
Duration (min)	2 yr	5 yr	10 yr	25 yr	50 yr	100 yr
60	39.65	52.29	60.65	71.22	79.06	86.85
120	26.54	36.07	42.38	50.36	56.27	62.15
360	11.59	15.46	18.03	21.27	23.67	26.05
720	6.79	8.77	10.08	11.73	12.96	14.17
1440	3.88	5.03	5.79	6.76	7.47	8.18

ECHO-G_A1B	Return Periods, T yrs					
Duration (min)	2 yr	5 yr	10 yr	25 yr	50 yr	100 yr
60	34.85	48.38	57.33	68.65	77.05	85.39
120	22.18	30.94	36.74	44.06	49.49	54.89
360	9.48	13.10	15.49	18.52	20.77	23.00
720	5.53	7.56	8.90	10.60	11.86	13.11
1440	3.16	4.26	4.99	5.91	6.60	7.28

ECHO-G_B1	Return Periods, T yrs					
Duration (min)	2 yr	5 yr	10 yr	25 yr	50 yr	100 yr
60	34.35	49.95	60.28	73.33	83.02	92.63
120	21.54	30.52	36.47	43.98	49.55	55.08
360	9.29	12.90	15.29	18.30	20.54	22.76
720	5.36	7.48	8.89	10.67	11.99	13.30
1440	3.04	4.15	4.89	5.82	6.52	7.20

ECHO-G_A2	Return Periods, T yrs					
Duration (min)	2 yr	5 yr	10 yr	25 yr	50 yr	100 yr
60	34.49	49.16	58.87	71.14	80.25	89.28
120	22.29	31.94	38.34	46.41	52.41	58.36
360	9.58	13.19	15.58	18.60	20.84	23.06
720	5.59	7.46	8.69	10.25	11.41	12.55
1440	3.24	4.21	4.86	5.68	6.28	6.89

GFDLCM2.1_A1B	Return Periods, T yrs					
Duration (min)	2 yr	5 yr	10 yr	25 yr	50 yr	100 yr
60	32.50	44.43	52.33	62.31	69.72	77.07
120	20.75	27.68	32.27	38.07	42.38	46.65
360	9.14	11.98	13.85	16.23	17.99	19.74
720	5.60	7.23	8.32	9.69	10.70	11.71
1440	3.20	4.10	4.69	5.45	6.00	6.56

GFDLCM2.1_B1	Return Periods, T yrs					
Duration (min)	2 yr	5 yr	10 yr	25 yr	50 yr	100 yr
60	33.63	48.66	58.61	71.18	80.51	89.77
120	21.32	30.52	36.61	44.31	50.02	55.68
360	9.22	13.30	15.99	19.40	21.92	24.43
720	5.61	7.92	9.45	11.38	12.82	14.24
1440	3.20	4.45	5.28	6.33	7.11	7.88

GFDLCM2.1_A2	Return Periods, T yrs					
Duration	2 yr	5 yr	10 yr	25 yr	50 yr	100 yr
60	31.88	44.60	53.02	63.65	71.54	79.38
120	20.29	28.65	34.17	41.16	46.34	51.48
360	8.98	12.54	14.90	17.89	20.10	22.29
720	5.37	7.33	8.63	10.26	11.48	12.68
1440	3.08	4.20	4.94	5.88	6.57	7.26

GISSAOM_A1B	Return Periods, T yrs					
Duration (min)	2 yr	5 yr	10 yr	25 yr	50 yr	100 yr
60	32.64	45.34	53.75	64.37	72.25	80.08
120	21.91	32.53	39.55	48.43	55.02	61.56
360	9.23	13.52	16.36	19.95	22.61	25.25
720	5.40	7.56	9.00	10.81	12.16	13.49
1440	3.08	4.24	5.01	5.98	6.70	7.41

GISSAOM_B1	Return Periods, T yrs					
Duration (min)	2 yr	5 yr	10 yr	25 yr	50 yr	100 yr
60	29.39	39.40	46.03	54.41	60.62	66.78
120	19.40	27.11	32.21	38.66	43.45	48.20
360	8.13	11.05	12.99	15.44	17.25	19.05
720	4.91	6.35	7.30	8.50	9.40	10.28
1440	2.80	3.61	4.15	4.83	5.34	5.84

MIROC3HIRES_A1B	Return Periods, T yrs					
Duration (min)	2 yr	5 yr	10 yr	25 yr	50 yr	100 yr
60	28.29	39.68	47.22	56.74	63.81	70.82
120	18.04	24.66	29.05	34.59	38.70	42.78
360	7.86	10.31	11.92	13.97	15.48	16.99
720	4.78	6.20	7.13	8.32	9.19	10.06
1440	2.72	3.54	4.07	4.75	5.26	5.76

MIROC3HIRES_B1	Return Periods, T yrs					
Duration (min)	2 yr	5 yr	10 yr	25 yr	50 yr	100 yr
60	32.24	44.09	51.93	61.84	69.20	76.49
120	20.89	30.13	36.26	43.99	49.73	55.43
360	8.77	12.33	14.69	17.67	19.88	22.07
720	5.17	6.88	8.01	9.44	10.50	11.56
1440	2.98	3.91	4.53	5.31	5.89	6.47

MIROC3MEDRES_A1B	Return Periods, T yrs					
Duration (min)	2 yr	5 yr	10 yr	25 yr	50 yr	100 yr
60	27.16	39.84	48.24	58.85	66.72	74.54
120	17.30	25.17	30.38	36.97	41.86	46.71
360	7.75	11.26	13.58	16.51	18.69	20.84
720	4.65	6.70	8.06	9.77	11.04	12.31
1440	2.70	3.75	4.45	5.34	5.99	6.64

MIROC3MEDRES_B1	Return Periods, T yrs					
Duration (min)	2 yr	5 yr	10 yr	25 yr	50 yr	100 yr
60	31.13	43.16	51.13	61.20	68.67	76.09
120	19.90	27.66	32.79	39.28	44.09	48.87
360	8.58	11.64	13.66	16.21	18.11	19.99
720	5.15	6.77	7.83	9.18	10.18	11.17
1440	2.94	3.78	4.35	5.05	5.58	6.10

MIROC3MEDRES_A2	Return Periods, T yrs					
Duration (min)	2 yr	5 yr	10 yr	25 yr	50 yr	100 yr
60	24.12	34.15	40.79	49.17	55.40	61.57
120	15.18	20.15	23.44	27.59	30.67	33.73
360	6.75	8.91	10.35	12.16	13.50	14.83
720	4.28	5.59	6.45	7.55	8.36	9.17
1440	2.49	3.20	3.66	4.25	4.69	5.13

CCSRNIES_B21	Return Periods, T yrs					
Duration (min)	2 yr	5 yr	10 yr	25 yr	50 yr	100 yr
60	40.08	57.19	68.52	82.84	93.46	104.01
120	25.63	38.11	46.37	56.81	64.55	72.24
360	10.93	15.56	18.62	22.49	25.36	28.21
720	6.36	8.70	10.26	12.22	13.67	15.11
1440	3.62	4.91	5.75	6.83	7.62	8.41

CSIROMK2b_B11	Return Periods, T yrs					
Duration (min)	2 yr	5 yr	10 yr	25 yr	50 yr	100 yr
60	26.68	39.56	48.09	58.86	66.86	74.79
120	17.63	26.21	31.89	39.08	44.40	49.69
360	7.29	10.59	12.78	15.53	17.58	19.61
720	4.19	5.89	7.02	8.45	9.51	10.56
1440	2.35	3.25	3.85	4.60	5.16	5.71

APEPNDIX E: IDF Plots of Selected Scenarios
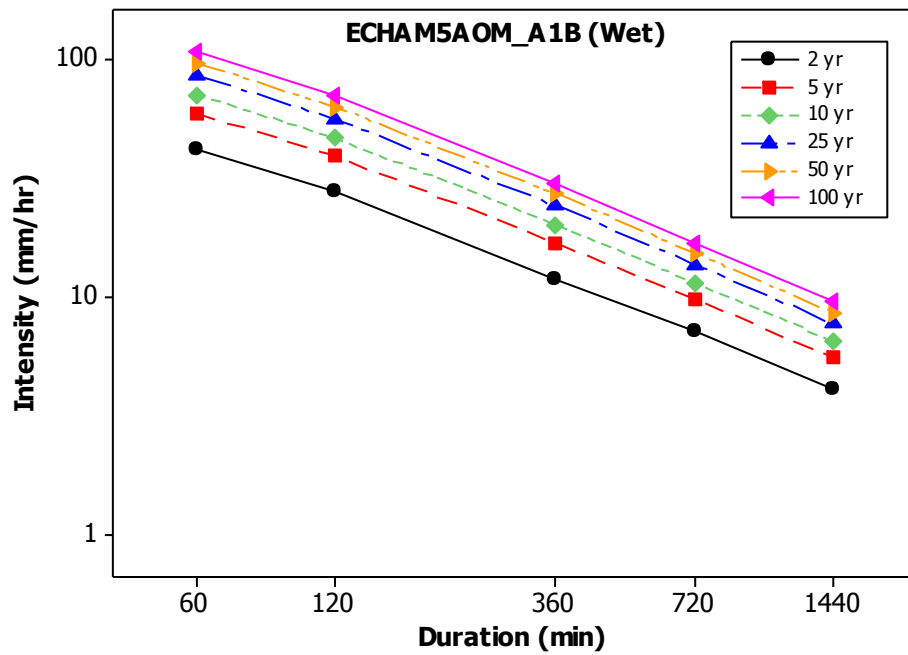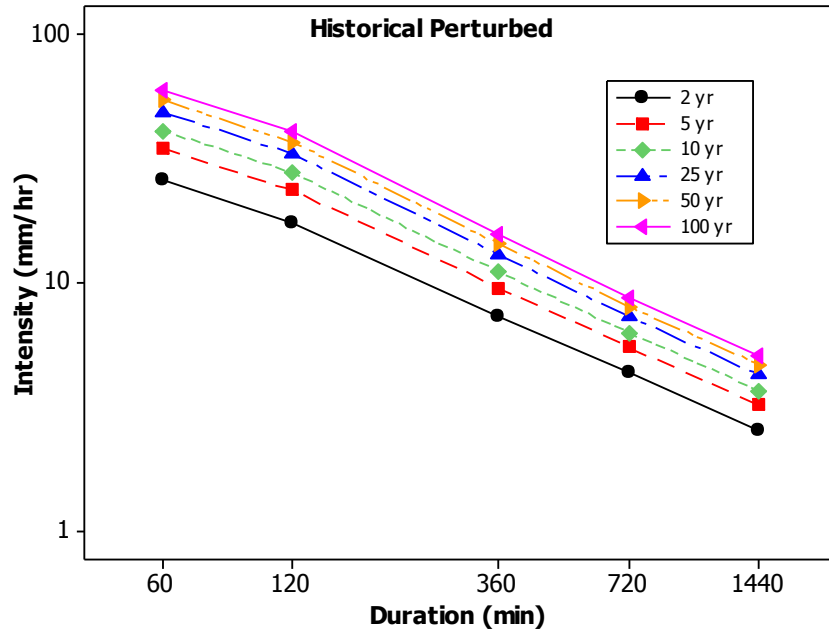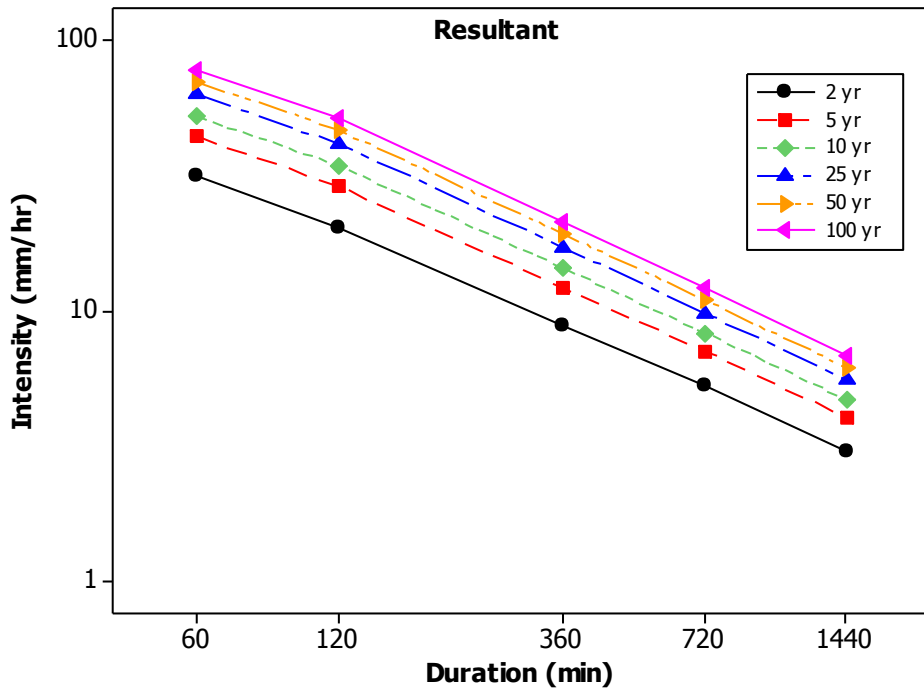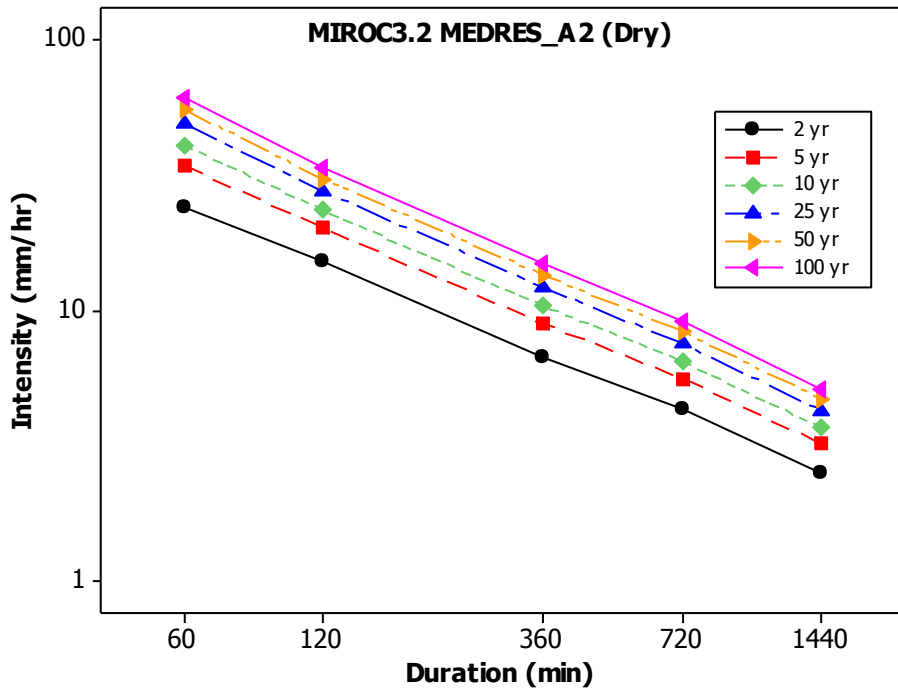
APPENDIX F: Previous Reports in the Series

(1) Slobodan P. Simonovic (2001). Assessment of the Impact of Climate Variability and Change on the Reliability, Resiliency and Vulnerability of Complex Flood Protection Systems. Water Resources Research Report no. 038, Facility for Intelligent Decision Support, Department of Civil and Environmental Engineering, London, Ontario, Canada, 91 pages. ISBN: (print) 978-0-7714-2606-3; (online) 978-0-7714-2607-0.

(2) Predrag Prodanovic (2001). Fuzzy Set Ranking Methods and Multiple Expert Decision Making. Water Resources Research Report no. 039, Facility for Intelligent Decision Support, Department of Civil and Environmental Engineering, London, Ontario, Canada, 68 pages. ISBN: (print) 978-0-7714-2608-7; (online) 978-0-7714-2609-4.

(3) Nirupama and Slobodan P. Simonovic (2002). Role of Remote Sensing in Disaster Management. Water Resources Research Report no. 040, Facility for Intelligent Decision Support, Department of Civil and Environmental Engineering, London, Ontario, Canada, 107 pages. ISBN: (print) 978-0-7714-2610-0; (online) 978-0-7714- 2611-7.

(4) Taslima Akter and Slobodan P. Simonovic (2002). A General Overview of Multiobjective Multiple-Participant Decision Making for Flood Management. Water Resources Research Report no. 041, Facility for Intelligent Decision Support, Department of Civil and Environmental Engineering, London, Ontario, Canada, 65 pages. ISBN: (print) 978-0-7714-2612-4; (online) 978-0-7714-2613-1.

(5) Nirupama and Slobodan P. Simonovic (2002). A Spatial Fuzzy Compromise Approach for Flood Disaster Management. Water Resources Research Report no. 042, Facility for Intelligent Decision Support, Department of Civil and Environmental Engineering, London, Ontario, Canada, 138 pages. ISBN: (print) 978-0-7714-2614-8; (online) 978-0-7714-2615-5.

(6) K. D. W. Nandalal and Slobodan P. Simonovic (2002). State-of-the-Art Report on Systems Analysis Methods for Resolution of Conflicts in Water Resources Management. Water Resources Research Report no. 043, Facility for Intelligent Decision Support, Department of Civil and Environmental Engineering, London, Ontario, Canada, 216 pages. ISBN: (print) 978-0-7714-2616-2; (online) 978-0-7714-2617-9.

(7) K. D. W. Nandalal and Slobodan P. Simonovic (2003). Conflict Resolution Support System – A Software for the Resolution of Conflicts in Water Resource Management. Water Resources Research Report no. 044, Facility for Intelligent Decision Support, Department of Civil and Environmental Engineering, London, Ontario, Canada, 144 pages. ISBN: (print) 978-0-7714-2618-6; (online) 978-0-7714-2619-3.

(8) Ibrahim El-Baroudy and Slobodan P. Simonovic (2003). New Fuzzy Performance Indices for Reliability Analysis of Water Supply Systems. Water Resources Research Report no. 045, Facility for Intelligent Decision Support, Department of Civil and Environmental Engineering, London, Ontario, Canada, 90 pages. ISBN: (print) 978-0-7714-2620-9; (online) 978-0-7714-2621-6.

(9) Juraj Cunderlik (2003). Hydrologic Model Selection for the CFCAS Project: Assessment of Water Resources Risk and Vulnerability to Changing Climatic Conditions. Water Resources Research Report no. 046, Facility for Intelligent Decision Support, Department of Civil and Environmental Engineering, London, Ontario, Canada, 40 pages. ISBN: (print) 978-0-7714-2622-3; (online) 978-0-7714- 2623-0.

(10) Juraj Cunderlik and Slobodan P. Simonovic (2004). Selection of Calibration and Verification Data for the HEC-HMS Hydrologic Model. Water Resources Research Report no. 047, Facility for Intelligent Decision Support, Department of Civil and Environmental Engineering, London, Ontario, Canada, 29 pages. ISBN: (print) 978-0-7714-2624-7; (online) 978-0-7714-2625-4.

(11) Juraj Cunderlik and Slobodan P. Simonovic (2004). Calibration, Verification and Sensitivity Analysis of the HEC-HMS Hydrologic Model. Water Resources Research Report no. 048, Facility for Intelligent Decision Support, Department of Civil and Environmental Engineering, London, Ontario, Canada, 113 pages. ISBN: (print) 978- 0-7714-2626-1; (online) 978-0-7714-2627-8.

(12) Predrag Prodanovic and Slobodan P. Simonovic (2004). Generation of Synthetic Design Storms for the Upper Thames River basin. Water Resources Research Report no. 049, Facility for Intelligent Decision Support, Department of Civil and Environmental Engineering, London, Ontario, Canada, 20 pages. ISBN: (print) 978- 0-7714-2628-5; (online) 978-0-7714-2629-2.

(13) Ibrahim El-Baroudy and Slobodan P. Simonovic (2005). Application of the Fuzzy Performance Indices to the City of London Water Supply System. Water Resources Research Report no. 050, Facility for Intelligent Decision Support, Department of Civil and Environmental Engineering, London, Ontario, Canada, 137 pages. ISBN: (print) 978-0-7714-2630-8; (online) 978-0-7714-2631-5.

(14) Ibrahim El-Baroudy and Slobodan P. Simonovic (2006). A Decision Support System for Integrated Risk Management. Water Resources Research Report no. 051, Facility for Intelligent Decision Support, Department of Civil and Environmental Engineering, London, Ontario, Canada, 146 pages. ISBN: (print) 978-0-7714-2632-2; (online) 978-0-7714-2633-9.

(15) Predrag Prodanovic and Slobodan P. Simonovic (2006). Inverse Flood Risk Modelling of The Upper Thames River Basin. Water Resources Research Report no. 052, Facility for Intelligent Decision Support, Department of Civil and Environmental Engineering, London, Ontario, Canada, 163 pages. ISBN: (print) 978-0-7714-2634-6; (online) 978-0-7714-2635-3.

(16) Predrag Prodanovic and Slobodan P. Simonovic (2006). Inverse Drought Risk Modelling of

The Upper Thames River Basin. Water Resources Research Report no. 053, Facility for Intelligent Decision Support, Department of Civil and Environmental Engineering, London, Ontario, Canada, 252 pages. ISBN: (print) 978-0-7714-2636-0; (online) 978-0-7714-2637-7.

(17) Predrag Prodanovic and Slobodan P. Simonovic (2007). Dynamic Feedback Coupling of Continuous Hydrologic and Socio-Economic Model Components of the Upper Thames River Basin. Water Resources Research Report no. 054, Facility for Intelligent Decision Support, Department of Civil and Environmental Engineering, London, Ontario, Canada, 437 pages. ISBN: (print) 978-0-7714-2638-4; (online) 978-0-7714-2639-1.

(18) Subhankar Karmakar and Slobodan P. Simonovic (2007). Flood Frequency Analysis Using Copula with Mixed Marginal Distributions. Water Resources Research Report no. 055, Facility for Intelligent Decision Support, Department of Civil and Environmental Engineering, London, Ontario, Canada, 144 pages. ISBN: (print) 978-0-7714-2658-2; (online) 978-0-7714-2659-9.

(19) Jordan Black, Subhankar Karmakar and Slobodan P. Simonovic (2007). A Web-Based Flood Information System. Water Resources Research Report no. 056, Facility for Intelligent Decision Support, Department of Civil and Environmental Engineering, London, Ontario, Canada, 133 pages. ISBN: (print) 978-0-7714-2660-5; (online) 978-0-7714-2661-2.

(20) Angela Peck, Subhankar Karmakar and Slobodan P. Simonovic (2007). Physical, Economical, Infrastructural and Social Flood Risk – Vulnerability Analyses in GIS. Water Resources Research Report no. 057, Facility for Intelligent Decision Support, Department of Civil and Environmental Engineering, London, Ontario, Canada, 80 pages. ISBN: (print) 978-0-7714-2662-9; (online) 978-0-7714-2663-6.

(21) Predrag Prodanovic and Slobodan P. Simonovic (2007). Development of Rainfall Intensity Duration Frequency Curves for the City of London Under the Changing Climate. Water Resources Research Report no. 058, Facility for Intelligent Decision Support, Department of Civil and Environmental Engineering, London, Ontario, Canada, 51 pages. ISBN: (print) 978-0-7714-2667-4; (online) 978-0-7714-2668-1.

(22) Evan G. R. Davies and Slobodan P. Simonovic (2008). An integrated system dynamics model for analyzing behaviour of the social-economic-climatic system: Model description and model use guide. Water Resources Research Report no. 059, Facility for Intelligent Decision Support, Department of Civil and Environmental Engineering, London, Ontario, Canada, 233 pages. ISBN: (print) 978-0-7714-2679-7; (online) 978-0-7714-2680-3.

(23) Vasan Arunachalam (2008). Optimization Using Differential Evolution. Water Resources Research Report no. 060, Facility for Intelligent Decision Support, Department of Civil and Environmental Engineering, London, Ontario, Canada, 42 pages. ISBN: (print) 978-0-7714-2689-6; (online) 978-0-7714-2690-2.

(24) Rajesh Shrestha and Slobodan P. Simonovic (2009). A Fuzzy Set Theory Based Methodology for Analysis of Uncertainties in Stage-Discharge Measurements and Rating Curve. Water Resources Research Report no. 061, Facility for Intelligent Decision Support, Department

of Civil and Environmental Engineering, London, Ontario, Canada, 104 pages. ISBN: (print) 978-0-7714-2707-7; (online) 978-0-7714-2708-4.

(25) Hyung-Il Eum, Vasan Arunachalam and Slobodan P. Simonovic (2009). Integrated Reservoir Management System for Adaptation to Climate Change Impacts in the Upper Thames River Basin. Water Resources Research Report no. 062, Facility for Intelligent Decision Support, Department of Civil and Environmental Engineering, London, Ontario, Canada, 81 pages. ISBN: (print) 978-0-7714-2710-7; (online) 978-0-7714-2711-4.

(26) Evan G. R. Davies and Slobodan P. Simonovic (2009). Energy Sector for the Integrated System Dynamics Model for Analyzing Behaviour of the Social- Economic-Climatic Model. Water Resources Research Report no. 063. Facility for Intelligent Decision Support, Department of Civil and Environmental Engineering, London, Ontario, Canada. 191 pages. ISBN: (print) 978-0-7714-2712-1; (online) 978-0-7714-2713-8.

(27) Leanna King, Tarana Solaiman, and Slobodan P. Simonovic (2009). Assessment of Climatic Vulnerability in the Upper Thames River Basin. Water Resources Research Report no. 064, Facility for Intelligent Decision Support, Department of Civil and Environmental Engineering, London, Ontario, Canada, 61pages. ISBN: (print) 978-0-7714-2816-6; (online) 978-0-7714-2817-3.

(28) Slobodan P. Simonovic and Angela Peck (2009). Updated Rainfall Intensity Duration Frequency Curves for the City of London under Changing Climate. Water Resources Research Report no. 065, Facility for Intelligent Decision Support, Department of Civil and Environmental Engineering, London, Ontario, Canada, 64pages. ISBN: (print) 978-0-7714-2819-7; (online) 987-0-7714-2820-3.

(29) Leanna King, Tarana Solaiman, and Slobodan P. Simonovic (2010). Assessment of Climatic Vulnerability in the Upper Thames River Basin: Part 2. Water Resources Research Report no. 066, Facility for Intelligent Decision Support, Department of Civil and Environmental Engineering, London, Ontario, Canada, 72pages. ISBN: (print) 978-0-7714-2834-0; (online) 978-0-7714-2835-7.

(30) Christopher J. Popovich, Slobodan P. Simonovic and Gordon A. McBean (2010).Use of an Integrated System Dynamics Model for Analyzing Behaviour of the Social-Economic-Climatic System in Policy Development. Water Resources Research Report no. 067, Facility for Intelligent Decision Support, Department of Civil and Environmental Engineering, London, Ontario, Canada, 37 pages. ISBN: (print) 978-0-7714-2838-8; (online) 978-0-7714-2839-5.

(31) Hyung-Il Eum and Slobodan P. Simonovic (2009). City of London: Vulnerability of Infrastructure to Climate Change; Background Report 1 – Climate and Hydrologic Modeling. Water Resources Research Report no. 068, Facility for Intelligent Decision Support, Department of Civil and Environmental Engineering, London, Ontario, Canada, 102pages. ISBN: (print) 978-0-7714-2844-9; (online) 978-0-7714-2845-6.

(32) Dragan Sredojevic and Slobodan P. Simonovic (2009). City of London: Vulnerability of Infrastructure to Climate Change; Background Report 2 – Hydraulic Modeling and Floodplain Mapping. Water Resources Research Report no. 069, Facility for Intelligent Decision Support, Department of Civil and Environmental Engineering, London, Ontario, Canada, 147 pages. ISBN: (print) 978-0-7714-2846-3; (online) 978-0-7714-2847-0.

(33) Tarana A. Solaiman and Slobodan P. Simonovic (February 2011). Quantifying Uncertainties in the Modelled Estimates of Extreme Precipitation Events at the Upper Thames River Basin. Water Resources Research Report no. 070, Facility for Intelligent Decision Support, Department of Civil and Environmental Engineering, London, Ontario, Canada, 167 pages. ISBN: (print) 978-0-7714-2878-4; (online) 978-0-7714-2880-7.

(34) Tarana A. Solaiman and Slobodan P. Simonovic (January 2011). Assessment of Global and Regional Reanalyses Data for Hydro-Climatic Impact Studies in the Upper Thames River Basin. Water Resources Research Report no. 071, Facility for Intelligent Decision Support, Department of Civil and Environmental Engineering, London, Ontario, Canada, 74 pages. ISBN: (print) 978-0-7714-2892-0; (online) 978-0-7714-2899-9.